

# Towards Out-of-Distribution Detection with Divergence Guarantee in Deep Generative Models

Yufeng Zhang, Wanwei Liu, Zhenbang Chen, Ji Wang, Zhiming Liu, Kenli Li, Hongmei Wei

**Abstract**—Recent research has revealed that deep generative models including flow-based models and Variational autoencoders may assign higher likelihoods to out-of-distribution (OOD) data than in-distribution (ID) data. However, we cannot sample out OOD data from the model. This counterintuitive phenomenon has not been satisfactorily explained. In this paper, we prove theorems to investigate the divergences in flow-based model and give two explanations to the above phenomenon from divergence and geometric perspectives, respectively. Our theoretical analysis inspires us to detect OOD data by Kullback-Leibler divergence between the distribution of representations and prior. Furthermore, we decompose the KL divergence to improve our group-wise anomaly detection method and support point-wise anomaly detection as well. We have conducted experiments on prevalent benchmarks to evaluate our method. Experimental results demonstrate the superiority of our OOD detection method.

**Index Terms**—Out-of-distribution detection, flow-based model, Kullback-Leibler divergence.

## 1 INTRODUCTION

ANOMALY detection is the process of “finding patterns in data that do not conform to expected behavior” [1]. Anomaly detection can be classified into group anomaly detection (GAD) [2] and point-wise anomaly detection (PAD) [1], [3]. In unsupervised learning setting, the model is trained on a set of unlabeled data  $\{x_1, \dots, x_n\}$  which are drawn independently from an unknown distribution  $p^*$ . GAD is to determine whether a group of test inputs  $\{\tilde{x}_1, \dots, \tilde{x}_m\} (m > 1)$  are drawn from  $p^*$ . When  $m = 1$ , GAD becomes PAD. Examples of GAD include discovering high-energy particle physics, [4], anomalous galaxy clusters in astronomy [5], [6], unusual vorticity in fluid dynamics [7], and stealthy attacks [2], [8]. Examples of PAD include detecting intrusion [1], fraud [9], malware [10], and medical anomalies [1]. In literature, the term anomaly is also referred to as outlier, peculiarity, out-of-distribution (OOD) data, etc. In the following, we mainly use the term *OOD data* as in the most related works.

In this paper, we focus on unsupervised OOD detection using deep generative models (DGM) including flow-based model and VAE. Recent research shows that deep generative models (DGMs) including flow-based models

[11], [12], VAE [13], and auto-regressive models [14], [15] are not capable of distinguishing OOD data from training data (or in-distribution (ID) data) according to the model likelihood [16], [17], [18], [19], [20], [21]. For example, as shown in Figure 1(b), and 1(c), Glow [11] assigns higher likelihoods for SVHN (MNIST) when trained on CIFAR-10 (FashionMNIST). However, as pointed by Nalisnick *et al.* [20] *we cannot sample out OOD data although they are assigned higher likelihood.* Another similar phenomenon is observed in class conditional Glow (GlowGMM), which contains a Gaussian Mixture Model on the top layer with one Gaussian for each class [11], [22], [23]. GlowGMM does not achieve the same performance as prevalent discriminative models (*e.g.*, ResNet [24]) on FashionMNIST. This means that one component may assign higher likelihoods for other classes. As shown in Figure 7 in the supplementary material, these centroids are closer than we imagine. However, *we always sample out images of the correct class from the corresponding component.*

Nalisnick *et al.* explain the above phenomenon by the discrepancy of the typical set and high probability density regions of the model distribution [20]. They propose using typicality test to detect OOD data. However, their explanation and method fail on problems where the likelihoods of ID and OOD data coincide (*e.g.*, CIFAR-10 vs CIFAR-100, CelebA vs CIFARs).

In this paper, we try to answer the following two questions:

- Q1: Why cannot sample out new data similar to OOD data set in flow-based model? We need a unified answer to this question whenever OOD data have lower, higher, or coinciding likelihoods.
- Q2: How to detect OOD data using flow-based model and VAE without supervision?

We start our research from the sampling process. Flow-based model constructs diffeomorphism from visible space

- Yufeng Zhang and Kenli Li are with the College of Computer Science and Electronic Engineering, Hunan University, Changsha, China.  
E-mail: yufengzhang@hnu.edu.cn, lkl@hnu.edu.cn
- Wanwei Liu, Zhenbang Chen and Ji Wang are with the College of Computer Science, National University of Defense Technology, Changsha, China.  
E-mail: wwliu@nudt.edu.cn, zbchen@nudt.edu.cn, wj@nudt.edu.cn
- Zhiming Liu is with the Centre for Intelligent and Embedded Software, Northwest Polytechnical University, Taicang, and Centre for Research and Innovation in Software Engineering, Southwest University, Chongqing, China.  
E-mail: zliu@nwpu.edu.cn
- Hongmei Wei is with the Department of Computer Science & Engineering, Shanghai Jiao Tong University, Shanghai, China.  
E-mail: wei-hong-mei@sjtu.edu.cn

Manuscript received xx xx, 2021; revised xx xx, 2021.

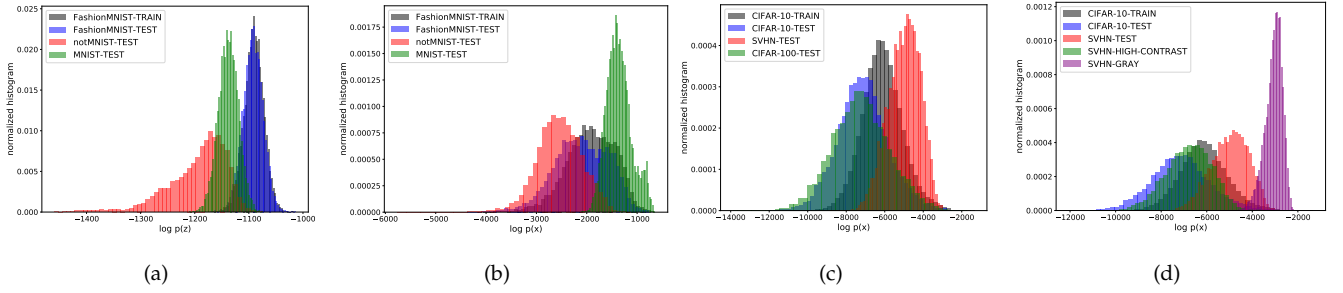


Fig. 1. Distribution of likelihoods of ID data set (train and test) and OOD data set. (a) and (b) show the normalized histogram of  $\log p(z)$  and  $\log p(x)$  on Glow trained on FashionMNIST, respectively. (c) shows the normalized histogram of  $\log p(x)$  on Glow trained on CIFAR-10. (d) shows that  $\log p(x)$  of OOD data can be manipulated by adjusting the contrast of images. SVHN-HIGH-CONTRAST and SVHN-GRAY are SVHN with adjusted contrast by a factor of 2.0 and 0.3, respectively.

to latent space. Each input data point is mapped to a unique representation in latent space. So we should ask why we cannot sample out the representations of OOD data from prior. In this paper, we first answer Q1 and then propose a unified OOD detection method.

The contributions of this paper are:

- 1) We prove several theorems to investigate the divergences in flow-based model. Based on these theorems, we attempt to provide a theoretical guarantee for OOD detection method.
- 2) We give two answers to Q1 from two perspectives. The first answer reveals the large divergence between the distribution of representations of OOD data and the prior. The second answer states that the representations of OOD data locate in specific directions.
- 3) Our answer to Q1 prompts us to perform GAD according to the Kullback-Leibler (KL) divergence between the distribution of representations and prior. However, estimating KL divergence is hard when OOD data set is arbitrary. Luckily, we observe that, for a wide range of problems, the representations of OOD data set in flow-based model follow a Gaussian-like distribution. This allows us to use the fitted Gaussian in KL divergence estimation and makes the whole method easy to perform. We also find that the same criterion works even better when the representations of OOD data set do not follow Gaussian-like distribution.
- 4) Furthermore, we decompose the KL divergence between the distribution of representations and prior to improve GAD method and support PAD. We split representations into multiple groups to implement our improvement. We also devise a splitting strategy that can leverage the local pixel dependence of representations.
- 5) We conduct experiments to evaluate our method. The results demonstrate the effectiveness, robustness, and generality of our method. For GAD, our method achieves near 100% AUROC for almost all the problems encountered in the experiments and is robust against data manipulations. On the contrary, the state-of-the-art (SOTA) GAD method is not better than random guessing on challenging problems and can be attacked by data manipulation in almost all cases. For PAD, our method also outperforms the baseline.

The remaining part of this paper is organized as follows. Section 2 gives the background and proposes data manipulations to attack the SOTA methods. Section 3 presents

our theoretical analysis to answer Q1. Section 4 shows the details of our OOD detection method. Section 5 reports evaluation results. Section 6 discusses more details of our method. Section 7 discusses related work. Finally, Section 8 concludes.

## 2 PROBLEM SETTINGS

### 2.1 Background

**Flow-based generative model** constructs diffeomorphism  $f$  from visible space  $\mathcal{X}$  to latent space  $\mathcal{Z}$  [11], [12], [25], [26]. The model uses a series of diffeomorphisms implemented by multilayered neural networks

$$\mathbf{x} \xleftrightarrow{f_1} \mathbf{h}_1 \xleftrightarrow{f_2} \mathbf{h}_2 \dots \xleftrightarrow{f_n} \mathbf{z} \quad (1)$$

like flow. The whole bijective transformation  $f(\mathbf{x}) = f_n \circ f_{n-1} \dots f_1(\mathbf{x})$  can be seen as encoder, and the inverse function  $f^{-1}(\mathbf{z})$  is used as decoder. According to the change of variable rule, the probability density function of the model can be formulated as

$$\begin{aligned} \log p_{\mathcal{X}}(\mathbf{x}) &= \log p_{\mathcal{Z}}(f(\mathbf{x})) + \log \left| \det \frac{\partial \mathbf{z}}{\partial \mathbf{x}^T} \right| \\ &= \log p_{\mathcal{Z}}(f(\mathbf{x})) + \sum_{i=1}^n \log \left| \det \frac{\partial \mathbf{h}_i}{\partial \mathbf{h}_{i-1}^T} \right| \end{aligned} \quad (2)$$

where  $\mathbf{x} = \mathbf{h}_0$ ,  $\mathbf{z} = \mathbf{h}_n$ ,  $\frac{\partial \mathbf{h}_i}{\partial \mathbf{h}_{i-1}^T}$  is the Jacobian of  $f_i$ ,  $\det$  is the determinant.

Here prior  $p_{\mathcal{Z}}(\mathbf{z})$  is chosen as tractable density function. For example, the most popular prior is standard Gaussian  $\mathcal{N}(0, I)$ , which makes  $\log p_{\mathcal{Z}}(\mathbf{z}) = -(1/2) \times \sum_i \mathbf{z}_i^2 + C$  ( $C$  is a constant). After training, one can sample noise  $\varepsilon$  from prior and generate new samples  $f^{-1}(\varepsilon)$ .

**Variational Autoencoder (VAE)** is directed graphical model approximating the data distribution  $p(\mathbf{x})$  with encoder-decoder architecture. The probabilistic encoder  $q_{\phi}(\mathbf{z}|\mathbf{x})$  approximates the unknown intractable posterior  $p(\mathbf{z}|\mathbf{x})$ . The probabilistic decoder  $p_{\theta}(\mathbf{x}|\mathbf{z})$  approximates  $p(\mathbf{x}|\mathbf{z})$ . In VAE, the variational lower bound of the marginal likelihood of data points (ELBO)

$$\begin{aligned} \mathcal{L}(\theta, \phi) &= \frac{1}{N} \sum_{i=1}^N E_{\mathbf{z} \sim q_{\phi}} [\log p_{\theta}(\mathbf{x}^i|\mathbf{z})] - KL(q_{\phi}(\mathbf{z}|\mathbf{x}^i)||p(\mathbf{z})) \end{aligned} \quad (3)$$

can be optimized using stochastic gradient descent. After training, one can sample  $\mathbf{z}$  from prior  $p(\mathbf{z})$  and use the decoder  $p_{\theta}(\mathbf{x}|\mathbf{z})$  to generate new samples.

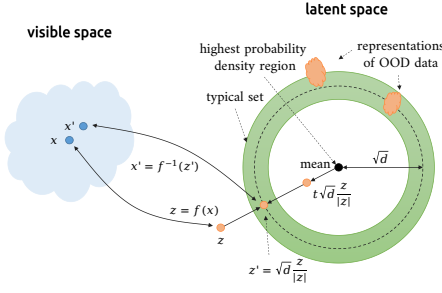


Fig. 2. Typical set of  $d$ -dimensional standard Gaussian is an annulus with radius  $\sqrt{d}$ . We can encode an input  $x$  into  $z$ , rescale  $z$  to the typical set as  $z' = \sqrt{d}z/|z|$ , and then decode  $z'$  as  $x'$ . The resulting image is similar to the original one.

## 2.2 Attacking Likelihood

In [20], Nalisnick *et al.* conjecture that the counterintuitive phenomena in Q1 stem from the distinction of high probability density regions and the typical set of the model distribution [18], [20]. For example, Figure 2 shows the typical set of  $d$ -dimensional standard Gaussian, which is an annulus with a radius of  $\sqrt{d}$  [27]. When sampling from the Gaussian, it is highly likely to get points in the typical set. Neither the highest density region (*i.e.* the center) nor the lowest density region far from the mean would be reached. Based on this explanation, Nalisnick *et al.* propose using typicality test (Ty-test in short) to detect OOD data and achieve SOTA GAD results [20]. However, their explanation and method do not apply to problems where OOD data reside in the typical set of model distribution.

In the following, we show how to manipulate OOD data set to make the likelihood distribution of ID and OOD dataset coincide.

**M1: rescaling  $z$  to typical set of prior.** We train Glow with 768-dimensional standard Gaussian prior on FashionMNIST. Figure 1(a) shows the histogram of log-likelihood of representations under prior ( $\log p(z)$ ). Note that  $\log p(z)$  of FashionMNIST are around  $-768 \times (0.5 \times \ln 2\pi e) \approx -1089.74$ , which is the log-probability of typical set of the prior [28]. Here it seems hopeful to detect OOD data by  $p(z)$  or typicality test in the latent space [18]. However, as shown in Figure 2, we can decode each OOD data point  $x$  as  $z = f(x)$  and rescale  $z$  to the typical set by setting  $z' = \sqrt{d} \times z/|z|$  ( $d = 768$ ). Then we decode  $z'$  to generate image  $x' = f^{-1}(z')$ . We find that  $z'$  corresponds to the similar image with  $z$ . Figure 8 in supplementary material shows some examples of  $f^{-1}(z')$ . These results demonstrate that flow-based model is not able to expel representations of OOD data from the typical set of the prior. To the best of our knowledge, we are the first to discover that the latents rescaled to typical set of prior still can be mapped back to legal images.

**M2: adjusting contrast.** Figure 1(b) shows that Glow trained on FashionMNIST assigns higher (lower)  $p(x)$  for MNIST (notMNIST). Ty-test can handle problems where the expectations of  $p(x)$  of inputs and training set diverge (*e.g.*, FashionMNIST vs MNIST/notMNIST) [20]. However, when the likelihoods of ID and OOD data sets coincide, Ty-test fails (*e.g.*, CIFAR-10 vs CIFAR-100 in Glow, Figure 1(c)). Nalisnick *et al.* also find that the likelihood distribution can

be manipulated by adjusting the variance of inputs [16]. As shown in Figure 1(d), SVHN with increased contrast by a factor of 2.0 has coinciding likelihood distribution with CIFAR-10 on Glow trained on CIFAR-10. So it is impossible to detect OOD data by  $p(x)$  or typicality test on the model distribution. In our experiments, we can manipulate the likelihoods of OOD data set in this way for almost all problems. See Figure 9~12 in the supplementary material for details. Besides, some more complicated likelihood-based methods, *e.g.*, likelihood ratio, can also be affected by such manipulation (see Section 5). Similarly, in VAE, we can also manipulate the likelihood distribution by adjusting the contrast of input images.

In summary, we can manipulate both  $p(x)$  and  $p(z)$  of OOD data without the knowledge of the parameters of the model. In Section 5, we will show that our method is robust to the above manipulations.

## 2.3 Problems

We use ID vs OOD to represent an OOD detection problem and use “ID (OOD) representations” to denote representations of ID (OOD) data. According to the behavior of OOD data set, we group OOD detection problems into two categories:

- *Category I:* OOD data set has smaller or similar variance with ID data set and tends to have higher or similar likelihoods;
- *Category II:* OOD data set has larger variance than ID data and tends to have lower likelihoods.

As shown in the subsection 2.2, it is easy to use M2 to convert one problem from one category to another. In this paper, we present a unified OOD detection method for both categories.

## 3 THEORETICAL ANALYSIS

In subsection 3.1, we first give several theorems that help to investigate the divergence between the distributions in flow-based model. Then in subsection 3.2 we give answers to Q1 from two perspectives.

### 3.1 Theorems

**Large Divergence Guaranteed.** In our analysis, we use  $(h, \phi)$ -divergence family which includes many commonly used divergence measures in machine learning fields [29] (*e.g.*, the KL divergence, Jensen-Shannon divergence, and squared Hellinger distance, see Section A in the supplementary material for details).

**Theorem 1** *Given a flow-based model  $z = f(x)$  with prior  $p_Z^r$ . Suppose that  $X_1 \sim p_X(x)$ ,  $X_2 \sim q_X(x)$ ,  $Z_1 = f(X_1) \sim p_Z(z)$  and  $Z_2 = f(X_2) \sim q_Z(z)$ . Let  $D_\phi^h$  be a  $(h, \phi)$ -divergence measure,  $D$  be a proper statistical distance metric belonging to the  $(h, \phi)$ -divergence family, and  $\mathcal{R}_D$  be the range of  $D$ .*

- $D_\phi^h(p_X, q_X) = D_\phi^h(p_Z, q_Z)$  holds [30].*
- For any  $0 < d < \sup(\mathcal{R}_D)$ , there are  $d' > 0$  and  $\epsilon > 0$  so that  $D(q_Z, p_Z^r) > d$  when  $D(p_X, q_X) > d'$  and  $D(p_Z, p_Z^r) < \epsilon$ .*

**Proof** (a) Since  $D_\phi^h(p, q) = h(D_\phi(p, q))$ , where  $D_\phi(p, q)$  is  $\phi$ -divergence between  $p$  and  $q$ , it suffices to prove

$D_\phi(p_X, q_X) = D_\phi(p_Z, q_Z)$ . It has been known that diffeomorphism preserves  $\phi$ -divergence. See [30] for the proof.

- (b) Since  $D$  is a proper statistical distance metric and satisfies the triangle inequality, we have  $D(p_Z, p_Z^r) + D(q_Z, p_Z^r) \geq D(p_Z, q_Z)$ . For any  $d > 0$  and  $\epsilon > 0$ , if  $D(p_Z, q_Z) > d + \epsilon = d'$  and  $D(p, p_Z^r) < \epsilon$ , we have  $D(q_Z, p_Z^r) > d$ . Since  $D$  belongs to the  $(h, \phi)$ -divergence family, from Theorem 1a we know  $D(p_X, q_X) = D(p_Z, q_Z)$ . Thus we have Theorem 1b.  $\square$

**Note.** The proof of Theorem 1 relies on diffeomorphisms. According to the Brouwer Invariance of Domain Theorem [31],  $R^n$  cannot be homeomorphic to  $R^m$  if  $n \neq m$ . So Theorem 1 does not apply to non-diffeomorphisms (e.g., vanilla VAE). The Brouwer Invariance of Domain Theorem also implies that there is no dead neuron in flow-based model. Otherwise, we can construct diffeomorphism from high to low dimensional space.

Theorem 1 provides a general perspective for investigating the divergences between distributions in flow-based model. Currently, flow-based models are usually trained by maximum likelihood estimation, which is equivalent to minimizing the forward KL divergence  $KL(p_X(\mathbf{x})||p_X^r(\mathbf{x}))$  [26], [32], where  $p_X(\mathbf{x})$  is the distribution of training data and  $p_X^r(\mathbf{x})$  is the model distribution. However, KL divergence is not symmetric. The difference between forward and reverse KL divergence of two distributions can be any large. We cannot apply Theorem 1b on KL divergence directly.

The following theorems 2 ~ 4 use a famous transcendental function, the Lambert  $W$  function.

**Definition 1 Lambert  $W$  Function** [33], [34]. The reverse function of function  $y = xe^x$  is called Lambert  $W$  function  $y = W(x)$ .

When  $x \in \mathbb{R}$ ,  $W$  is a multivalued function with two branches  $W_0, W_{-1}$ , where  $W_0$  is the principal branch (also called branch 0) and  $W_{-1}$  is the branch  $-1$ .

**Approximate symmetry of small KL divergence between Gaussians.** The following Theorem 2 guarantees that the KL divergence between two  $n$ -dimensional Gaussians  $KL(\mathcal{N}_1||\mathcal{N}_2)$  is small when  $KL(\mathcal{N}_2||\mathcal{N}_1)$  is small.

**Theorem 2** Let  $KL$  be the Kullback-Leibler divergence,  $\epsilon$  be a positive real number,  $W_0$  be the principal branch of the Lambert  $W$  Function. For any  $n$ -dimensional Gaussians  $\mathcal{N}(\boldsymbol{\mu}_1, \boldsymbol{\Sigma}_1)$  and  $\mathcal{N}(\boldsymbol{\mu}_2, \boldsymbol{\Sigma}_2)$ , if  $KL(\mathcal{N}(\boldsymbol{\mu}_1, \boldsymbol{\Sigma}_1)||\mathcal{N}(\boldsymbol{\mu}_2, \boldsymbol{\Sigma}_2)) \leq \epsilon$ , then

$$KL(\mathcal{N}(\boldsymbol{\mu}_2, \boldsymbol{\Sigma}_2)||\mathcal{N}(\boldsymbol{\mu}_1, \boldsymbol{\Sigma}_1)) \leq \frac{1}{2} \left\{ \frac{1}{-W_0(-e^{-(1+2\epsilon)})} - \log \frac{1}{-W_0(-e^{-(1+2\epsilon)})} - 1 \right\} \quad (4)$$

**Proof** The proof is too long to be included in the same paper. The details of the proof are presented in our work [35], which is submitted independently to another venue.

**Notes.** The supremum in Inequation 4 is small when  $\epsilon$  is small. See Table 10 in the supplementary material for some approximate values of the supremum. Besides, it needs strict conditions to make Inequality 4 tight. In machine learning practice, KL divergence is usually much smaller than the supremum. See our proof in [35] for details.

The following Theorem 3 gives the infimum of  $KL(\mathcal{N}_1||\mathcal{N}_2)$  when  $KL(\mathcal{N}_1||\mathcal{N}_2) \geq M$  for  $M > 0$ .

**Theorem 3** Let  $KL$  be the Kullback-Leibler divergence,  $M > 0$  be a positive real number,  $W_{-1}$  be the branch  $-1$  of the Lambert  $W$  Function. For any two  $n$ -dimensional Gaussians  $\mathcal{N}(\boldsymbol{\mu}_1, \boldsymbol{\Sigma}_1)$  and  $\mathcal{N}(\boldsymbol{\mu}_2, \boldsymbol{\Sigma}_2)$ , if  $KL(\mathcal{N}(\boldsymbol{\mu}_1, \boldsymbol{\Sigma}_1)||\mathcal{N}(\boldsymbol{\mu}_2, \boldsymbol{\Sigma}_2)) \geq M$ , then

$$KL(\mathcal{N}(\boldsymbol{\mu}_2, \boldsymbol{\Sigma}_2)||\mathcal{N}(\boldsymbol{\mu}_1, \boldsymbol{\Sigma}_1)) \geq \frac{1}{2} \left\{ \frac{1}{-W_{-1}(-e^{-(1+2M)})} - \log \frac{1}{-W_{-1}(-e^{-(1+2M)})} - 1 \right\} \quad (5)$$

**Proof** Theorem 3 can be derived from Theorem 2 or proved independently. See our work [35] for the proof.

**Relaxed triangle inequality of KL divergence between Gaussians.** The following Theorem 4 shows that the KL divergence between Gaussians follows a relaxed triangle inequality.

**Theorem 4** Let  $KL$  be the Kullback-Leibler divergence,  $W_0$  and  $W_{-1}$  be the branches 0,  $-1$  of the Lambert  $W$  Function, respectively. For any three  $n$ -dimensional Gaussians  $\mathcal{N}(\boldsymbol{\mu}_1, \boldsymbol{\Sigma}_1)$ ,  $\mathcal{N}(\boldsymbol{\mu}_2, \boldsymbol{\Sigma}_2)$  and  $\mathcal{N}(\boldsymbol{\mu}_3, \boldsymbol{\Sigma}_3)$ , if  $KL(\mathcal{N}(\boldsymbol{\mu}_1, \boldsymbol{\Sigma}_1)||\mathcal{N}(\boldsymbol{\mu}_2, \boldsymbol{\Sigma}_2)) \leq \epsilon_1$ ,  $KL(\mathcal{N}(\boldsymbol{\mu}_2, \boldsymbol{\Sigma}_2)||\mathcal{N}(\boldsymbol{\mu}_3, \boldsymbol{\Sigma}_3)) \leq \epsilon_2$ , then

$$KL(\mathcal{N}(\boldsymbol{\mu}_1, \boldsymbol{\Sigma}_1)||\mathcal{N}(\boldsymbol{\mu}_3, \boldsymbol{\Sigma}_3)) < \epsilon_1 + \epsilon_2 + \frac{1}{2} \left\{ W_{-1}(-e^{-(1+2\epsilon_1)})W_{-1}(-e^{-(1+2\epsilon_2)}) + W_{-1}(-e^{-(1+2\epsilon_1)}) + W_{-1}(-e^{-(1+2\epsilon_2)}) + 1 - W_{-1}(-e^{-(1+2\epsilon_2)}) \left( \sqrt{2\epsilon_1} + \sqrt{\frac{2\epsilon_2}{-W_0(-e^{-(1+2\epsilon_2)})}} \right)^2 \right\} \quad (6)$$

**Proof** The proof is too long to be included in the same paper. See our work [35] for details.

Most importantly, all the bounds in Theorem 2, 3, and 4 are independent of the dimension  $n$ . So these theorems can be applied to high-dimensional problems (e.g., flow-based model).

### 3.2 Why Cannot Sample Out OOD Data?

Based on the theorems we have proven, we can give two explanations on why cannot sample out OOD data from two perspectives.

#### 3.2.1 Divergence Perspective

Figure 3 illustrates how we can apply Theorem 1 to investigate the divergences between the following distributions: the distributions of ID data ( $p_X(\mathbf{x})$ ) and OOD data ( $q_X(\mathbf{x})$ ), the distributions of ID representations ( $p_Z(\mathbf{z})$ ) and OOD representations ( $q_Z(\mathbf{z})$ ), the prior  $p_Z^r(\mathbf{z})$ , and the model induced distribution  $p_X^r(\mathbf{x})$  such that  $Z_r \sim p_Z^r(\mathbf{z})$  and  $X_r = f^{-1}(Z_r) \sim p_X^r(\mathbf{x})$ . In the following, we first discuss the general case. Then we conduct further analysis for one category of problems.

**1. General case.** Our analysis consists of the following steps.

- **Step 1:** In practice, ID and OOD datasets are sampled from different distributions. Take KL divergence  $KL(p_X(\mathbf{x})||q_X(\mathbf{x})) = \int p_X(\mathbf{x}) \log \frac{p_X(\mathbf{x})}{q_X(\mathbf{x})} d\mathbf{x}$  as an example. When each input  $\mathbf{x}$  belongs to only one dataset,  $KL(p_X(\mathbf{x})||q_X(\mathbf{x}))$  can be considered as any large.

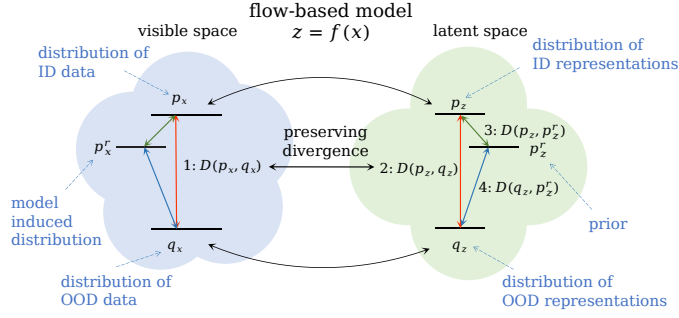


Fig. 3. This figure shows the divergences between several distributions in flow-based model, where  $D(p, q)$  is KL divergence between  $p$  and  $q$ . 1. In visible space,  $p_X, q_X$  and  $p_X^r$  are unknown. The only thing we can confirm is the (KL) divergence between  $p_X$  and  $q_X$  is large. 2. According to Theorem 1, flow-based model preserves  $(h, \phi)$ -divergence. So we know the (KL) divergence between  $p_Z$  and  $q_Z$  is large too. 3. Flow-based model is trained to has a small  $D(p_Z, p_Z^r)$ . 4. According to our analysis, we can know  $D(q_Z, p_Z^r)$  is large.

Therefore, it is natural to consider the following assumption for any divergence measure.

**Assumption 1** *The distributions of ID and OOD data are far from each other.*

- **Step 2:** We can suppose the model is expressible enough and trained by maximum likelihood estimation. This is equal to minimizing forward KL divergence  $KL(p_X || p_X^r)$  [26]. According to Theorem 1, we have  $KL(p_X || p_X^r) = KL(p_Z || p_Z^r)$ , so  $KL(p_Z || p_Z^r)$  is small.
- **Step 3:** However, KL divergence is not symmetric. It might happens that  $KL(p || q)$  is small but  $KL(q || p)$  is very large. Luckily, we observe in flow-based models ID representations manifest strong normality. We perform generalized Shapiro-Wilk test for multivariate normality [36]. Table 1 shows the results. We can see that ID representations always have high  $p$ -values. Based on the above observation, we can use a Gaussian  $\mathcal{N}_p$  to approximate  $p_Z$  and have  $KL(p_Z || p_Z^r) \approx KL(\mathcal{N}_p || p_Z^r)$ . Now we can apply Theorem 2 on  $KL(\mathcal{N}_p || p_Z^r)$  and know that reverse KL divergence  $KL(p_Z^r || \mathcal{N}_p)$  is small. Therefore,  $KL(p_Z^r || p_Z)$  is small too. In a nutshell, we can consider the second assumption.

**Assumption 2** *The distribution of ID representations and the prior are close enough.*

- **Step 4:** Now that both the forward and reverse KL divergence are small, we can assume  $p_Z \approx p_Z^r$  and have  $KL(q_Z || p_Z^r) \approx KL(q_Z || p_Z)$ . In step 1, we have known  $KL(q_X || p_X) = KL(q_Z || p_Z)$  is large, so  $KL(q_Z || p_Z^r)$  is large too. This leads to an answer to Q1 from the divergence perspective.

**Answer 1 to Q1:** The distribution of OOD representations is far from the prior regardless of when the likelihoods of OOD data are higher, lower, or coinciding with that of ID data.

**Notes.** Both Assumption 1 and 2 are reasonable in

practice. In **Step 4** we assume  $p_Z \approx p_Z^r$ . Here we do not require a precise approximation. This is because  $KL(q_Z || p_Z)$  is large enough in practice. Take SVHN vs CIFAR-10 for example, each data point belongs to only one dataset. So  $KL(q_Z || p_Z)$  can be assumed any large. Such precondition allows us to use an imprecise approximation in  $p_Z \approx p_Z^r$ .

**2. The Gaussian case.** We also perform normality test on OOD representations. The results are surprising. As shown in Table 1, OOD representations in all *Category I* problems except for SVHN vs Constant have  $p$ -values greater than 0.05. As far as we know, we are the first to observe this phenomenon (More details are presented in section 4.1.1). In summary, we have the following key observation.

**Key observation:** ID representations of flow-based models follow Gaussian-like distribution. For *Category I* problems, the representations of OOD dataset tend to follow Gaussian-like distribution.

Using our theorems on the properties of KL divergence between Gaussians, we can conduct further analysis when  $q_Z$  is Gaussian-like. We can use a Gaussian  $\mathcal{N}_q$  to approximate  $q_Z$  and have  $KL(q_Z || p_Z^r) \approx KL(\mathcal{N}_q || p_Z^r)$ ,  $KL(p_Z || \mathcal{N}_q) \approx KL(p_Z || q_Z)$ . Now we know that  $KL(p_Z || q_Z)$  is large and  $KL(p_Z || p_Z^r)$  is small. According to the relaxed triangle inequality in Theorem 4,  $KL(p_Z^r || \mathcal{N}_q)$  must not be small. Furthermore, we can apply Theorem 3 on  $KL(p_Z^r || \mathcal{N}_q)$  and know that  $KL(\mathcal{N}_q || p_Z^r)$  is large. Finally, we know  $KL(q_Z || p_Z^r)$  is large too.

### 3.2.2 Geometric Perspective

Theorem 5 decomposes forward KL divergence into two parts. It provides a basis for further analysis.

**Theorem 5** *Let  $X \sim p_X^*(\mathbf{x})$  be an  $n$ -dimensional random vector,  $X_i \sim p_{X_i}^*(x)$  be the  $i$ -th dimensional element of  $X$ . Then*

$$KL(p_X^*(\mathbf{x}) || \mathcal{N}(0, I_n)) \quad (7)$$

$$= \underbrace{KL(p_X^*(\mathbf{x}) || \prod_{i=1}^n p_{X_i}^*(x))}_{I_d[p_X^*] \text{ total correlation}} + \underbrace{\sum_{i=1}^n KL(p_{X_i}^*(x) || \mathcal{N}(0, 1))}_{D_d[p_X^*] = \sum_{i=1}^n D_d[p_{X_i}^*] \text{ dimensional-wise KL divergence}} \quad (8)$$

**Proof**

$$\begin{aligned} & KL(p_X^*(\mathbf{x}) || \mathcal{N}(0, I_n)) \\ &= \mathbb{E}_{p_X^*(\mathbf{x})} \left[ \log \left( \frac{p_X^*(\mathbf{x})}{\mathcal{N}(0, I_n)} \right) \right] \\ &= \mathbb{E}_{p_X^*(\mathbf{x})} \left[ \log \left( \frac{p_X^*(\mathbf{x})}{\prod_{i=1}^n p_{X_i}^*(x)} \cdot \frac{\prod_{i=1}^n p_{X_i}^*(x)}{\mathcal{N}(0, I_n)} \right) \right] \\ &= \mathbb{E}_{p_X^*(\mathbf{x})} \left[ \log \left( \frac{p_X^*(\mathbf{x})}{\prod_{i=1}^n p_{X_i}^*(x)} \right) \right] + \mathbb{E}_{p_X^*(\mathbf{x})} \left[ \log \left( \frac{\prod_{i=1}^n p_{X_i}^*(x)}{\mathcal{N}(0, 1)} \right) \right] \\ &= \mathbb{E}_{p_X^*(\mathbf{x})} \left[ \log \left( \frac{p_X^*(\mathbf{x})}{\prod_{i=1}^n p_{X_i}^*(x)} \right) \right] + \mathbb{E}_{p_X^*(\mathbf{x})} \left[ \sum_{i=1}^n \log \left( \frac{p_{X_i}^*(x)}{\mathcal{N}(0, 1)} \right) \right] \\ &= \mathbb{E}_{p_X^*(\mathbf{x})} \left[ \log \left( \frac{p_X^*(\mathbf{x})}{\prod_{i=1}^n p_{X_i}^*(x)} \right) \right] + \sum_{i=1}^n \mathbb{E}_{p_{X_i}^*(x)} \left[ \log \left( \frac{p_{X_i}^*(x)}{\mathcal{N}(0, 1)} \right) \right] \\ &= KL(p_X^*(\mathbf{x}) || \prod_{i=1}^n p_{X_i}^*(x)) + \sum_{i=1}^n KL(p_{X_i}^*(x) || \mathcal{N}(0, 1)) \end{aligned}$$

□



TABLE 1

Results of Generalized Shapiro-Wilk test for multivariate normality on the representations of datasets under Glow. See Section 5.1 for the explanation of data set names. The larger  $W$  and  $p$  are, the more Gaussian-like the distribution is. When  $p \geq 0.05$ , there is no evidence to reject the normality hypothesis. In our experiments, ID representations under all models manifest strong normality. For *Category I* problems, all OOD representations except for SVHN vs Constant manifest normality.

ID	Input(ID/OOD)	Category	$W$	$p$ -value
Fashion.	<b>Fashion.</b>	-	0.9996	<b>0.9479</b>
	Constant	I	0.9992	<b>0.5872</b>
	Constant-C(0.1)	I	0.9995	<b>0.9212</b>
	MNIST	I	0.9985	<b>0.0733</b>
	MNIST-C(10.0)	I	0.9991	<b>0.4114</b>
	notMNIST	I	0.9989	<b>0.2337</b>
	notMNIST-C(0.005)	I	0.9993	<b>0.6411</b>
SVHN	<b>SVHN</b>	-	0.9993	<b>0.6227</b>
	Constant	I	0.9911	9.6e-10
	Constant-C(0.1)	I	0.9992	<b>0.5442</b>
	Uniform	II	0.9992	<b>0.5273</b>
	Uniform-C(0.008)	II	0.9993	<b>0.6203</b>
	CelebA	II	0.9336	< 2.2e-16
	CelebA-C(0.08)	I	0.9993	<b>0.6503</b>
	CIFAR-10	II	0.99429	5.7e-07
	CIFAR-10-C(0.12)	I	0.9995	<b>0.8838</b>
	CIFAR-100	II	0.9528	< 2.2e-16
	CIFAR-100-C(0.12)	I	0.9985	<b>0.0760</b>
	Imagenet32	II	0.8618	< 2.2e-16
CIFAR-10	Imagenet32-C(0.07)	I	0.9670	< 2.2e-16
	<b>CIFAR-10</b>	-	0.9995	<b>0.9064</b>
	Constant	I	0.9992	<b>0.5512</b>
	Constant-C(0.1)	I	0.9991	<b>0.4725</b>
	Uniform	I	0.70958	< 2.2e-16
	Uniform-C(0.02)	II	0.99931	<b>0.6964</b>
	CIFAR-100	I	0.9994	<b>0.8426</b>
	CelebA	I	0.9987	<b>0.1390</b>
	CelebA-C(0.3)	I	0.9994	<b>0.7960</b>
	Imagenet32	I	0.9977	0.0048
	TinyImagenet	I	0.9995	<b>0.3092</b>
	SVHN	I	0.9989	<b>0.2532</b>
CelebA	SVHN-C(2.0)	I	0.9989	<b>0.2547</b>
	<b>CelebA</b>	-	0.9992	<b>0.6064</b>
	Constant	I	0.9989	<b>0.2605</b>
	Constant-C(0.1)	I	0.9984	<b>0.7184</b>
	Uniform	II	0.9993	<b>0.6922</b>
	Uniform-C(0.012)	II	0.9992	<b>0.5815</b>
	CIFAR-10	I	0.9992	<b>0.5953</b>
	CIFAR-100	I	0.9990	<b>0.3313</b>
	Imagenet32	I	0.9993	<b>0.6410</b>
	Imagenet32-C(0.07)	I	0.9992	<b>0.5524</b>
	SVHN	I	0.9991	<b>0.4351</b>
	SVHN-C(1.8)	I	0.9990	<b>0.3600</b>

Theorem 5 decomposes forward KL divergence into two non-negative parts:  $I_d$  is total correlation (generalized mutual information) measuring the mutual dependence between dimensions [37];  $D_d$  is dimension-wise KL divergence containing the divergence between the marginal distribution of each dimension and prior. We use  $[p_X^*]$  to denote one term is computed from  $p_X^*$ .

Theorem 5 can help us to investigate the forward KL divergence further. For ID data, we have known that  $KL(p_Z(z)||p_Z^r(z))$  is small. According to Theorem 5,  $I_d[p_Z]$  is also small. This indicates that ID data tends to have independent representations. On the contrary, for OOD data, a large  $KL(q_Z(z)||p_Z^r(z))$  allows a large  $I_d[q_Z]$ . Although it is hard to estimate  $I_d[q_Z]$  [37], we can use an alternative dependence measure, *i.e.*, the most commonly used correlation coefficient, to investigate the linear dependency.

We train Glow on FashionMNIST and test on MNIST/notMNIST. Figure 4 shows the histogram of the non-diagonal elements in the correlation matrix of representations. We can see that OOD representations are more correlated. In

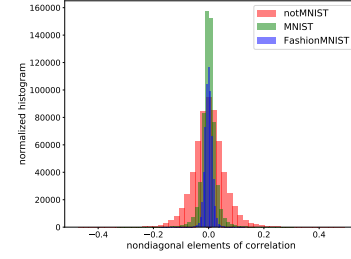


Fig. 4. Glow trained on FashionMNIST, tested on MNIST/notMNIST. Histogram of non-diagonal elements in the correlation coefficient of representations.

fact, this happens for all the problems in our experiments. See Figure 18 to 23 in supplementary material for more details. We note that correlation completely characterizes dependence only when data follows Gaussian distribution. In last subsection, we have shown that for *Category I* problems,  $q_Z$  tends to be Gaussian-like.

From a geometric perspective, a high correlation between dimensions indicates the representations of OOD data set locate in specific directions [38]. In high dimensional space, it is hard to obtain data on specific directions by sampling from standard Gaussian. When OOD representations reside in the typical set of prior, we can treat the phenomenon in Q1 as a manifestation of the curse of dimensionality.

Furthermore, we scale the norm of OOD representations with different factors. The decoded images also vary from ID data to OOD data gradually. See Figure 13 in the supplementary material for details.

Overall, this leads to the second answer to Q1.

**Answer 2 to Q1:** OOD representations locate in specific directions with specific norms. In high dimensional space, it is hard to sample out data in specific directions from prior regardless of whether these data reside in the typical set or not.

## 4 ANOMALY DETECTION METHOD

In this section, we first propose a preliminary GAD method. Then we improve the method to support small batch size and PAD.

### 4.1 A Preliminary GAD Method

Answer 1 reminds us to detect OOD data by estimating  $KL(p||p_Z^r)$ , where  $p$  is the distribution of representations of inputs. However, when only samples are available, divergence estimation is provable hard and the estimation error decays slowly in high dimension space [39], [40], [41]. This brings difficulty in applying existing divergence estimation [41], [42], [43], [44], [45] to high dimensional problems with small sample size. Luckily, as shown in Table 1, we observe that both ID data and OOD data of *Category I* problems follow Gaussian-like distribution. This provides us a facility to estimate the KL divergence for GAD.



Fig. 5. Glow trained on CIFAR-10. Generated images from prior (up), fitted Gaussian from representations of OOD dataset notMNIST (down).

#### 4.1.1 Flow-based Model

**ID data.** As discussed in Subsection 3.2, we can use a Gaussian  $\mathcal{N}_p$  to approximate  $p_Z$ . Here we use sample expectation  $\tilde{\mu}$  and covariance  $\tilde{\Sigma}$  of representations to estimate the parameters of  $\mathcal{N}_p$ <sup>1</sup>. Experiments also show that we can generate high-quality images by sampling from  $\mathcal{N}_p$  rather than the prior. Therefore, we have

$$\begin{aligned} & KL(p_Z || p_Z^r) \\ & \approx KL(\mathcal{N}_p(\tilde{\mu}, \tilde{\Sigma}) || \mathcal{N}(\mu, \Sigma)) \\ & = \frac{1}{2} \left\{ \log \frac{|\Sigma|}{|\tilde{\Sigma}|} + \text{Tr}(\Sigma^{-1} \tilde{\Sigma}) + (\mu - \tilde{\mu})^T \Sigma^{-1} (\mu - \tilde{\mu}) - n \right\} \end{aligned} \quad (9)$$

**OOD data in Category I problems.** At the very beginning, we observed that the fitted Gaussian from OOD representations contains style information of that dataset. We train Glow on CIFAR-10 and test on notMNIST (gray-scale images are preprocessed for consistency, see Section 5.1). Then we replace the prior with fitted Gaussian from representations of notMNIST and generate new images. Surprisingly, as shown in Figure 5, we find that the generated images seem similar to notMNIST, although the images are blurred. In this way, using a single Glow model, we can generate images with the style of multiple OOD datasets, including (not)MNIST, SVHN, CelebA, etc. See Figure 14~16 in the supplementary material for details. Such a similar phenomenon is also reported by [46], which is released contemporaneously with the first edition of this paper<sup>2</sup>.

Most importantly, these results remind us that  $q_Z$  may be also Gaussian-like to some extent. To validate this intuition, we perform generalized Shapiro-Wilk test for multivariate normality [47] on the representations. For each dataset, we randomly select 2000 inputs for normality test. As shown in Table 1, almost all OOD data sets of Category I problems have  $p$ -values greater than 0.05. It seems that OOD data sets “sitting inside of” the training data are also “Gaussianized” along with the training data.

Based on this observation, we can use fitted Gaussian  $\mathcal{N}_q$  to approximate  $q_Z$ . This allows us to use an expression to estimate  $KL(q_Z || p_Z^r)$ .

**OOD data in Category II problems.** Table 1 shows that OOD representations in Category II problems do not follow Gaussian-like distribution. Nevertheless, we find that Equation (9) performs even better on Category II problems.

When  $p_Z^r = \mathcal{N}(0, I)$ , Equation (9) equals to

$$\frac{1}{2} \left\{ -\log |\tilde{\Sigma}| + \text{Tr}(\tilde{\Sigma}) + \tilde{\mu}^T \tilde{\mu} - n \right\} \quad (10)$$

1. This is equal to using maximum likelihood estimation [32].

2. In [46], the authors only use the mean of fitted Gaussian, not including the covariance.

where generalized variance  $|\tilde{\Sigma}|$  and total variation  $\text{Tr}(\tilde{\Sigma})$  both measure the dispersion of all dimensions. So the first two items of Equation (10) compensate each other. For Category I problems, OOD representations are less dispersed than ID representations and have a larger  $-\log |\tilde{\Sigma}|$ . For Category II problems, OOD representations tend to be more dispersed, so  $\text{Tr}(\tilde{\Sigma})$  is larger. Besides, we find OOD representations always have a larger  $\tilde{\mu}^T \tilde{\mu}$  than ID representations.

In fact, when OOD representations do not follow Gaussian-like distributions, Equation (10) is a conservative criterion. The reason is revealed by the following theorem.

**Theorem 6** (see [48]) Let  $\mathcal{N}_1(\mu_1, \Sigma_1)$  and  $\mathcal{N}_1(\mu_2, \Sigma_2)$  be two  $n$ -dimensional Gaussian distributions. Assume that  $Z \sim P_Z(z)$  is an arbitrary  $n$ -dimensional continuous random variable with mean vector  $\mu_1$  and covariance matrix  $\Sigma_1$ , then

$$KL(\mathcal{N}_1(\mu_1, \Sigma_1) || \mathcal{N}_1(\mu_2, \Sigma_2)) \leq KL(P_Z(z) || \mathcal{N}_1(\mu_2, \Sigma_2)) \quad (11)$$

According to Theorem 6, Equation 10 computes a lower bound of  $KL(q_Z || p_Z^r)$ . If the criterion is large, then  $KL(q_Z || p_Z^r)$  must be large.

Overall, we get a preliminary answer to Q2.

**A preliminary answer to Q2:** Equation (10) can be used as a unified conservative criterion for GAD due to the following reasons.

- 1) For ID data, Equation (10) approximates  $KL(p_Z || p_Z^r)$  and should be small;
- 2) For OOD data whose representations follow Gaussian-like distribution, Equation (10) approximates  $KL(q_Z || p_Z^r)$  and should be large;
- 3) For OOD data whose representations do not follow Gaussian-like distribution, Equation (10) computes the lower bound of  $KL(q_Z || p_Z^r)$ . If the lower bound is large, then  $KL(q_Z || p_Z^r)$  must be large.

Besides, when batch size is too small to estimate the parameters, Equation (10) should be treated just as a statistic. Note that Equation (10) also applies to Gaussian prior with diagonal covariance  $\text{diag}(\sigma)$  and mean  $\mu$ . In such a case, we only need to normalize the data by a linear operation  $Z' = (Z - \mu)/\sigma$  while keeping  $KL(p_Z(z) || \mathcal{N}(\mu, \text{diag}(\sigma))) = KL(p_{Z'}(z) || \mathcal{N}(0, I))$  (by Theorem 1a). This equals to using Equation (9) directly. We also emphasize that we are not pursuing precise divergence estimation or parameter estimation, which are proven to be hard with very small batch sizes in high-dimensional problems.

#### 4.1.2 VAE

It is well-known that VAE and its variations learn independent representations [49], [50], [51], [52], [53]. In VAE, the probabilistic encoder  $q_\phi(z|x)$  is often chosen as Gaussian form  $\mathcal{N}(\mu(x), \text{diag}(\sigma(x)^2))$ , where  $z \sim q_\phi(z|x)$  is used as sampled representation,  $\mu(x)$  is used as mean representation. The KL term in variational evidence lower bound objective (ELBO) can be rewritten as  $E_{p(x)}[KL(q_\phi(z|x) || p(z))] = I(x; z) + KL(q(z) || p(z))$ , where  $p(z)$  is the prior,  $q(z)$  the aggregated posterior, and  $I(x; z)$  the mutual information between  $x$  and  $z$  [54]. Here the term  $KL(q(z) || p(z))$  pulls  $p_Z$

to the Gaussian prior and encourages independent sampled representations. We also investigate the representations in VAE. The results show that:

- 1) ID representations in VAE do not always have  $p$ -value greater than 0.05;
- 2) the representations of all OOD datasets do not have  $p$ -value greater than 0.05;
- 3) the sampled (mean) representations of OOD datasets are more correlated (see Figure 24~26 in the supplementary material).

Furthermore, there is no theoretical guarantee that  $KL(q_Z||p_Z^r)$  is large enough because Theorem 1 does not apply to non-diffeomorphisms.

We also tried the SOTA  $\phi$ -divergence estimation method applicable for VAE, i.e. RAM-MC [41]. Results show RAM-MC can also be affected by data manipulation **M2** (see Section 2.2) <sup>3</sup>. Finally, we find that Equation (10) also works for GAD with VAE.

## 4.2 Improvement

Up to now, we are still facing two challenges. Firstly, the performance of the preliminary GAD method tends to decrease when the batch size  $m$  is small (e.g.,  $m = 5$ ). Secondly, it seems impossible to apply our theorems to PAD because we cannot estimate the parameters from one single data point. In this section, we improve our preliminary method to tackle these two challenges. The key idea is splitting representation into groups.

### 4.2.1 Splitting Dimensions into Groups

The factorizability of standard Gaussian allows us to investigate representations in groups. Intuitively, if  $z \sim \mathcal{N}(0, I)$ , then each dimension group of  $z$  follows  $\mathcal{N}(0, I)$ ; Otherwise, it is unlikely that each part of  $z$  follows  $\mathcal{N}(0, I)$ . Thus, we can split one single  $z$  into multiple subvectors and investigate these subvectors separately. This also generates multiple samples from one data point artificially. Formally, we split random vector  $Z$  into  $k$   $l$ -dimensional ( $k = n/l$ ) subvectors  $\bar{Z}_1, \dots, \bar{Z}_k$ . We note the marginal distribution of  $\bar{Z}_i$  as  $p_{\bar{Z}_i}(z)$  ( $1 \leq i \leq k$ ). Then we can use the following Theorem 7 to decomposes  $KL(p_Z(z)||\mathcal{N}(0, I_n))$  further.

**Theorem 7** Let  $X \sim p_X^*(x)$  be an  $n$ -dimensional random vector. We note  $X = \bar{X}_1 \dots \bar{X}_k$  where  $\bar{X}_i \sim p_{\bar{X}_i}^*(x)$  be the  $i$ -th  $l$ -dimensional ( $k = n/l$ ) subvector of  $X$ ,  $\bar{X}_{ij} \sim p_{\bar{X}_{ij}}^*(x)$  be the  $j$ -th element of  $\bar{X}_i$ . Then,

$$\begin{aligned} & KL(p_X^*(x)||\mathcal{N}(0, I_n)) \\ &= \underbrace{KL(p_X^*(x)||\prod_{i=1}^k p_{\bar{X}_i}^*(x))}_{I_g[p_X^*]} + \underbrace{\sum_{i=1}^k KL(p_{\bar{X}_i}^*(x)||\mathcal{N}(0, I_l))}_{D_g[p_X^*]=\sum_{i=1}^k D_g[p_{\bar{X}_i}^*]} \quad (12) \\ &= \underbrace{KL(p_X^*(x)||\prod_{i=1}^k p_{\bar{X}_i}^*(x))}_{I_g[p_X^*]} + \underbrace{\sum_{i=1}^k KL(p_{\bar{X}_i}^*(x)||\prod_{j=1}^l p_{\bar{X}_{ij}}^*(x))}_{I_l[p_X^*]=\sum_{i=1}^k I_d^i[p_{\bar{X}_i}^*]} \end{aligned}$$

3. This does not prove that RAM-MC is not applicable to general-purpose divergence estimation.

$$+ \underbrace{\sum_{i=1}^n KL(p_{X_i}^*(z)||\mathcal{N}(0, 1))}_{D_d[p_X^*]} \quad (13)$$

**Proof** We can use the similar deduction in Theorem 5 and get Equation (12).

$$\begin{aligned} & KL(p_X^*(x)||\mathcal{N}(0, I_n)) \\ &= \mathbb{E}_{p_X^*(x)} \left[ \log \left( \frac{p_X^*(x)}{\prod_{i=1}^k p_{\bar{X}_i}^*(x)} \frac{\prod_{i=1}^k p_{\bar{X}_i}^*(x)}{\mathcal{N}(0, I_n)} \right) \right] \\ &= I_g[p_X^*] + D_g[p_X^*] \end{aligned}$$

Then we apply Theorem 5 on each  $D_g^i[p_{\bar{X}_i}^*]$  and have

$$\begin{aligned} & KL(p_{\bar{X}_i}^*(x)||\mathcal{N}(0, I_l)) \\ &= KL(p_{\bar{X}_i}^*(x)||\prod_{j=1}^l p_{\bar{X}_{ij}}^*(x)) + \sum_{j=1}^l KL(p_{\bar{X}_{ij}}^*(x)||\mathcal{N}(0, 1)) \quad (14) \end{aligned}$$

Finally, combining Equation (12) and 14 we can obtain Equation (13).  $\square$

In Equation (12),  $I_g$  is the generalized mutual information between dimension groups [37].  $D_g$  is group-wise KL divergence. Furthermore, in Equation (13)  $D_g$  is decomposed as  $I_l + D_d$ , where  $I_l$  is the generalized mutual information inside each group,  $D_d$  is dimension-wise KL divergence which also occurs in Equation (7). Combining Equation (7) and 13, we have  $I_d = I_g + I_l$  and  $D_g = I_l + D_d$ . Compared with Equation (7), Equation 12 distributes more divergence into the second part. When  $k = n$ , Equation (12) is equal to Equation (7).

Applying Theorem 7 on  $p_Z$  and  $q_Z$ , we get

$$\begin{aligned} KL(p_Z||p_Z^r) &= I_g[p_Z] + D_g[p_Z] = I_g[p_Z] + \sum_{i=1}^k D_g^i[p_{\bar{Z}_i}] \\ KL(q_Z||p_Z^r) &= I_g[q_Z] + D_g[q_Z] = I_g[q_Z] + \sum_{i=1}^k D_g^i[q_{\bar{Z}_i}] \end{aligned}$$

where  $p_{\bar{Z}_i}, q_{\bar{Z}_i}$  are the marginal distributions of subvectors of ID and OOD representations, respectively. In Section 3, we have known

$$I_g[q_Z] + D_g[q_Z] > I_g[p_Z] + D_g[p_Z] \quad (15)$$

Since  $I_g[p_Z] + D_g[p_Z]$  is small, we can assume that  $I_g[p_Z] < \varepsilon$ . To make Equation (15) hold, it suffices that  $D_g[q_Z] > D_g[p_Z] + \varepsilon$ . If the splitting strategy (see Section 4.2.2) distributes more divergence to  $D_g[q_Z]$  in Equation (12), it is high likely that  $D_g[q_Z] > D_g[p_Z]$ . Therefore, we can use  $D_g$  as the criterion to detect OOD data. The remaining problems are how to estimate  $D_g$  and how to choose a splitting strategy.

**Estimating  $D_g$ .** For ID data, we treat each representation as  $k$  data points sampled from a mixture of distributions  $p_{\bar{Z}_m}(z) = (1/k) \sum_{i=1}^k p_{\bar{Z}_i}(z)$  where  $p_{\bar{Z}_i}(1 \leq i \leq k)$  is very close to  $\mathcal{N}(0, I_k)$ . Thus, we can use a single Gaussian  $\mathcal{N}_{\bar{Z}_s}$  to approximate each  $p_{\bar{Z}_i}$ . Therefore,  $D_g[p_Z]$  can be approximated as

$$\begin{aligned} D_g[p_Z] &= \sum_{i=0}^k KL(p_{\bar{Z}_i}(z)||\mathcal{N}(0, I_l)) \\ &\approx k \times KL(\mathcal{N}_{\bar{Z}_s}||\mathcal{N}(0, I_l)) = k \times D_g[p_{\bar{Z}_s}] \end{aligned} \quad (16)$$



Now we can plug Equation (10) in Equation 16, except that each representation  $z$  is treated as  $k$  samples of  $p_{\bar{Z}_m}$ .

For OOD data, we cannot use a single Gaussian to approximate  $q_{\bar{Z}_m}(z) = (1/k) \sum_{i=1}^k q_{Z_i}(z)$  when  $q_{Z_i}(z)$  are far from each other or  $q_Z$  is not Gaussian-like. Nevertheless, we still can use Equation (10) as a statistic measuring the dispersion and deviation.

Finally, splitting representations not only makes PAD possible but also improve GAD performance because it increases the batch size artificially.

#### 4.2.2 Splitting Strategy: Leveraging Local Pixel Dependence

Our aim is to use  $D_g$  (Equation (16)) for OOD detection. When choosing the splitting strategy, we have the following two principles.

- 1) We should retain enough intragroup dependence in  $I_l[q_Z]$  to make  $D_g[q_Z] > D_g[p_Z] + \varepsilon$ ;
- 2) When the batch size is too small to estimate parameters, Equation (10) should still be a qualified statistic for OOD detection.

Take the Glow model for example, a representation  $z$  has shape  $(H \times W \times C)$  where  $H, W, C$  are the height, width, and the number of channels of  $z$ , respectively. The most natural choices are:

- 1)  $S1$ : split  $z$  as  $H \times W$   $C$ -dimensional vectors;
- 2)  $S2$ : split  $z$  as  $C$   $(H \times W)$ -dimensional vectors.

$S1$  retains inter-channel dependence into  $D_g$  while  $S2$  retains pixel dependence into  $D_g$ .

In Glow, the representation has shape  $(4 \times 4 \times 48)$ . The number of channels is much larger than the size of one channel. Our analysis of the correlation matrix also indicates that more divergence occurs between channels than that between pixels. So it seems that  $S1$  tends to have a larger  $I_l[q_Z]$ .

However, we find  $S2$  is better than  $S1$  especially when the batch size is small. The reason is that representations have simpler inter-channel dependence than pixel dependence as like natural images [55]. We split a single  $z$  into  $k$  subvectors  $z_1, \dots, z_k$ . Then we treat  $z_1, \dots, z_k$  as samples of one random vector  $\bar{Z}_m$  with multimodal distribution. If the  $r$ -th element  $\bar{Z}_{i,r}$  and  $s$ -th element  $\bar{Z}_{i,s}$  are strongly correlated for all  $1 \leq i \leq k$ , we can say that  $\bar{Z}_{m,r}$  and  $\bar{Z}_{m,s}$  are also strongly correlated. More generally, if  $\bar{Z}_1, \dots, \bar{Z}_k$  have the similar dependence structure,  $\bar{Z}_m$  would also has the similar dependence structure. Based on this intuition, we find that OOD representations manifest local pixel dependence. For example, we test CIFAR-10 and Imagenet32 on Glow trained on SVHN. For each OOD dataset, we visualize the correlation between pixels. As shown in Figure 27 in supplementary material, we find for almost all channels each pixel always has stronger correlation with its neighbors. Therefore, we can say that  $\bar{Z}_1, \dots, \bar{Z}_k$  tend to have a similar dependence structure. This means that using strategy  $S2$  tends to has a larger result when calculating Equation (10). On the contrary, when using strategy  $S1$  we cannot observe a similar dependence structure between channels. Therefore,  $S2$  is more suitable for PAD. The above analysis also applies to GAD with small batch size ( $2 \sim 5$ ).

Besides, we have also tried other splitting strategies. Evaluation results show that  $S2$  is the most stable and best one.

#### Algorithm 1 Anomaly Detection method (KLODS)

```

1: Input:  $f(x)$ : a well-trained flow-based model or the encoder of VAE using Gaussian prior  $\mathcal{N}(\mu, \text{diag}(\sigma))$ ;  $X = \{x_1, \dots, x_m\} (m \geq 1)$ : a batch of inputs;  $(H, W, C)$ : the shape of representations.  $t$ : threshold
2:  $\bar{Z} = \emptyset$ 
3: for  $i = 1$  to  $m$  do
4:    $z_i = f(x_i)$ 
5:    $z'_i = \frac{z_i - \mu}{\sigma}$ 
6:   split  $z'_i$  as  $C$   $(H \times W)$ -dimensional subvectors  $z'_{i,1} \dots z'_{i,C}$ 
7:    $\bar{Z} = \bar{Z} \cup \{z'_{i,1}, \dots, z'_{i,C}\}$ 
8: end for
9: compute sample covariance  $\tilde{\Sigma}$  and sample mean  $\tilde{\mu}$  of  $\bar{Z}$ 
10:  $c = (1/2) \{ -\log |\tilde{\Sigma}| + \text{tr}(\tilde{\Sigma}) + \tilde{\mu}^\top \tilde{\mu} - n \}$ 
11: if  $c > t$  then
12:   return "X is OOD data"
13: else
14:   return "X is ID data"
15: end if

```

Overall, we get an answer to Q2.

**Answer to Q2:** We use  $D_g$  (computed by Equation (16) and (10)) as a unified criterion for both GAD and PAD for flow-based models.

### 4.3 Algorithm

Algorithm 1 shows the details of our OOD detection method. Given inputs  $X = \{x_1, \dots, x_m\} (m \geq 1)$ , we compute the representations of each  $z_i = f(x_i)$  and split normalized  $z'_i = (z_i - \mu)/\sigma$  as  $C$   $(H \times W)$ -dimensional subvectors. Then we collect all the subvectors as  $\bar{Z}$  and use Equation (10) as the criterion. If  $c$  is greater than a threshold  $t$ , the input is determined as OOD data. Otherwise, the input is determined as ID data. Algorithm 1 becomes PAD when  $m = 1$ . We name our method as KLODS for *KL divergence-based Out-of-Distribution Detection with Splitted representations*.

Without splitting representations (line 6), Algorithm 1 can be used only for GAD. We call the algorithm without splitting representations as KLOD. Experimental results show that KLOD needs a larger batch size to achieve the same performance as KLODS for GAD.

## 5 EXPERIMENTS

We conduct experiments to evaluate the effectiveness, robustness, and generality of our OOD detection method.

### 5.1 Experimental Setting

**Benchmarks.** We evaluate our method with prevalent benchmarks in deep anomaly detection research [16], [17], [20], [56], [57], [58], including MNIST [59], FashionMNIST [60], notMNIST [61], CIFAR-10/100 [62], SVHN [63], CelebA [64], TinyImageNet [65], and ImageNet32 [66]. We also construct unnatural images as OOD data. *Constant* consists of images with all pixels equal to the same constant  $C \sim U\{0, 255\}$ .

*Uniform* consists of images with each pixel sampled independently from  $U\{0, 255\}$ . We also use the mixtures of different data sets as OOD data in GAD problems.

We use different dataset compositions falling into *Category I* and *Category II* problems. For example, CIFAR-10 vs SVHN falls into *Category I* and SVHN vs CIFAR-10 falls into *Category II*. All datasets are resized to  $32 \times 32 \times 3$  for consistency. For grayscale datasets of size  $28 \times 28 \times 1$ , we replicate channels and pad zeros around the image. We use  $S-C(k)$  ( $k \geq 0$ ) to denote dataset  $S$  with adjusted contrast by a factor  $k$ . See Figure 28 in the supplementary material for examples. The size of each test dataset is fixed to 10,000 for comparison.

**Models.** For flow-based model, we use OpenAI’s open-source implementation of Glow [67] with 768-dimensional standard Gaussian as prior except for CIFAR-10. For CIFAR-10, we use model checkpoint released by the authors of [20], [68] for fairness. The prior has learned mean and diagonal covariance. For VAE, we train convolutional VAE and use sampled representation for all problems. See Section C in the supplementary material for more details.

**Metrics.** We use threshold-independent metrics: area under the receiver operating characteristic curve (AUROC) and area under the precision-recall curve (AUPR) to evaluate our method [69]. We treat OOD data as positive data. For GAD, each dataset is shuffled and then divided into groups of size  $m$ . We compute AUROC and AUPR according to the portion of groups determined as OOD data.

**Baselines.** As far as we know, before this submission, there exist five methods that handle OOD data with higher likelihood in flow-based model under unsupervised setting.

- 1) WAIC [18]. In [20], Nalisnick *et al.* state that they were not able to replicate the results of WAIC. We also do not use WAIC as baseline.
- 2) typicality test in latent space [18]. In Section 2.2 we have shown typicality test in latent space can be attacked by data manipulation.
- 3) typicality test in model distribution (Ty-test) [20]. Ty-test is the only GAD method among the five methods. We use it as the baseline for GAD. Since Ty-test outperforms all other methods compared in [20], we do not use more baselines for GAD.
- 4) input complexity compensated likelihood [70]. We use this method as the baseline for PAD.
- 5) likelihood ratios [71]. In [70], Serrà *et al.* interpret their method as a likelihood-ratio test statistic and achieve better performance than method 5. Therefore, method 5 can be seen as an instance of method 4. Besides, the authors of method 5 did not report results on flow-based models. So we do not use method 5 as the baseline.

We run each method 5 times and show “mean $\pm$ std” for each problem.

## 5.2 Experimental Results

### 5.2.1 GAD Results

**KLODS on Unconditional Glow.** Table 2 shows the results of KLODS on Glow trained on FashionMNIST, SVHN, CIFAR-10, CelebA and tested on OOD datasets. We can see that our method outperforms the baseline. Specially, we adjust the contrast of OOD data set to make the likelihood distributions of ID and OOD data coincide. For these kinds

of problems, the performance of Ty-test degenerates severely. On the contrary, our method is much more robust against data manipulation. As reported by [20], CelebA vs CIFAR-10/100 is challenging for Ty-test. Our method can achieve 100% AUROC with batch size 10. We should point out that, although CelebA vs CIFAR-10/100 is not solved by the baseline method, our experimental results on CelebA vs others may be *not fair* for Ty-test. It is hard to make the likelihood distributions of CelebA train and test split fit well on the official Glow model <sup>4</sup> (see Figure 12 in the supplementary material for details). In principle, if the train and test split of ID data have coinciding likelihood distributions, the AUROC of Ty-test should not be less than around 50%. On the contrary, our GAD method is not affected by possible underfitting or overfitting.

Besides, KLODS outperforms Ty-test when batch size is smaller (*i.e.*,  $2 \sim 4$ ). See Table 11 in the supplementary material for details. Without splitting representations, KLOD needs a larger batch size than KLODS but still outperforms Ty-test. The results of KLOD are omitted.

**CIFAR-10 vs CIFAR-100** is one of the most challenging problems for Ty-test. KLOD and KLODS only achieve around 70% AUROC when batch size reaches 200. We argue the main reason is the model fails to capture the distribution of CIFAR-10 as other data sets. As shown in Figure 29 in the supplementary material, the model does not succeed to generate meaningful images. Thus,  $D(p_Z, p_Z^r)$  is not small enough and our theoretical analysis does not fit well in this situation. Currently, we are not aware of any unconditional flow-based model that can generate high-quality CIFAR-10-like images. We argue that it is meaningless to require an OOD detection method to achieve strong results on a failed generative model. In such a case, even the model itself generates “OOD data” that differ from the training set.

**Robustness.** The results presented above have demonstrated the robustness of our method against data manipulation method M2. KLODS achieves the same performance under M1 except that a slightly larger batch size (+5) is needed for CIFAR-10-related problems. The results are omitted for brevity.

**GAD on GlowGMM.** We train GlowGMM on Fashion-MNIST. For each component, we use learnable mean  $\mu_i$  and diagonal covariance  $\text{diag}(\sigma_i^2)$ . We treat each class as ID data and the rest classes as OOD data. As shown in Table 3, KLODS can achieve near 100% AUROC for all cases when batch size is 25. On the contrary, Ty-test is worse than random guessing in most cases.

It is clear that likelihood under each component is also not qualified for OOD detection. See Section D in the supplementary material for more details. Recent works have improved the accuracy of conditional Glow on classification problems [23], [72]. However, as long as GlowGMM does not achieve 100% classification accuracy, the question proposed in Section 1 remains.

**Generating OOD images using GlowGMM.** In Section 4.1, we have shown that unconditional Glow can generate blurred images like OOD data set with fitted Gaussian. In GlowGMM, we can generate *high-quality* OOD images with

4. We stop training after 2,000 epochs.

TABLE 2  
GAD Results of KLODS on Glow with batch sizes 5 and 10.

ID↓	OOD↓	Batch size→		$m=5$				$m=10$			
		Method→		KLODS		Ty-test		KLODS		Ty-test	
		Metric→		AUROC	AUPR	AUROC	AUPR	AUROC	AUPR	AUROC	AUPR
Fash.	Constant			100.0±0.0	100.0±0.0	42.1±0.3	42.1±0.2	100.0±0.0	100.0±0.0	41.7±0.5	41.9±0.2
	MNIST			99.8±0.0	99.8±0.0	97.6±0.1	95.8±0.5	100.0±0.0	100.0±0.0	99.7±0.1	99.6±0.1
	MNIST-C(10.0)			100.0±0.0	100.0±0.0	88.2±0.3	81.8±0.2	100.0±0.0	100.0±0.0	95.8±0.5	93.5±1.2
	notMNIST			100.0±0.0	100.0±0.0	77.5±0.3	74.6±0.4	100.0±0.0	100.0±0.0	87.1±0.2	85.4±0.4
	notMNIST-C(0.005)			100.0±0.0	100.0±0.0	25.0±0.6	35.8±0.2	100.0±0.0	100.0±0.0	23.8±0.4	35.5±0.1
SVHN	Constant			100.0±0.0	100.0±0.0	100.0±0.0	100.0±0.0	100.0±0.0	100.0±0.0	100.0±0.0	100.0±0.0
	Uniform			100.0±0.0	100.0±0.0	100.0±0.0	100.0±0.0	100.0±0.0	100.0±0.0	100.0±0.0	100.0±0.0
	Uniform-C(0.008)			100.0±0.0	100.0±0.0	13.5±0.5	33.0±0.1	100.0±0.0	100.0±0.0	11.1±0.5	32.6±0.1
	CelebA			100.0±0.0	100.0±0.0	100.0±0.0	100.0±0.0	100.0±0.0	100.0±0.0	100.0±0.0	100.0±0.0
	CelebA-C(0.08)			99.7±0.0	99.7±0.0	50.7±0.7	47.0±0.3	100.0±0.0	100.0±0.0	55.2±0.4	49.1±0.3
	CIFAR-10			100.0±0.0	100.0±0.0	100.0±0.0	100.0±0.0	100.0±0.0	100.0±0.0	100.0±0.0	100.0±0.0
	CIFAR-10-C(0.12)			97.0±0.2	97.4±0.2	31.6±0.5	37.9±0.2	99.3±0.1	99.4±0.1	25.0±0.3	35.6±0.1
	CIFAR-100			100.0±0.0	100.0±0.0	100.0±0.0	100.0±0.0	100.0±0.0	100.0±0.0	100.0±0.0	100.0±0.0
	CIFAR-100-C(0.12)			96.9±0.1	97.3±0.1	35.3±0.5	39.4±0.2	98.9±0.3	99.0±0.3	27.2±0.8	36.3±0.2
	ImageNet32			100.0±0.0	100.0±0.0	100.0±0.0	100.0±0.0	100.0±0.0	100.0±0.0	100.0±0.0	100.0±0.0
CIFAR-10	ImageNet32-C(0.07)			97.8±0.1	98.1±0.1	48.4±0.3	48.2±0.1	100.0±0.0	100.0±0.0	42.5±0.3	44.1±0.1
	Constant			100.0±0.0	100.0±0.0	100.0±0.0	100.0±0.0	100.0±0.0	100.0±0.0	100.0±0.0	100.0±0.0
	Uniform			100.0±0.0	100.0±0.0	100.0±0.0	100.0±0.0	100.0±0.0	100.0±0.0	100.0±0.0	100.0±0.0
	Uniform-C(0.02)			100.0±0.0	100.0±0.0	11.5±0.0	32.9±0.0	100.0±0.0	100.0±0.0	9.3±0.0	32.5±0.0
	CelebA			99.2±0.1	99.4±0.1	100.0±0.0	100.0±0.0	100.0±0.0	100.0±0.0	100.0±0.0	100.0±0.0
	CelebA-C(0.3)			84.3±0.3	84.4±0.4	28.4±0.5	36.7±0.2	94.5±0.3	94.7±0.3	23.5±0.5	35.2±0.1
	ImageNet32			90.0±0.2	92.1±0.1	99.2±0.1	99.3±0.1	95.0±0.4	96.2±0.2	100.0±0.0	100.0±0.0
	ImageNet32-C(0.3)			72.0±0.3	72.6±0.4	40.9±0.4	43.2±0.2	74.3±0.6	74.8±0.8	32.0±0.7	38.5±0.3
	SVHN			97.6±0.2	97.8±0.2	98.6±0.1	98.4±0.1	99.8±0.0	99.8±0.0	99.9±0.1	99.9±0.1
	SVHN-C(2.0)			100.0±0.0	100.0±0.0	33.5±0.4	61.0±0.2	100.0±0.0	100.0±0.0	27.2±0.5	58.2±0.1
CelebA	Constant			100.0±0.0	100.0±0.0	100.0±0.0	100.0±0.0	100.0±0.0	100.0±0.0	100.0±0.0	100.0±0.0
	Uniform			100.0±0.0	100.0±0.0	100.0±0.0	100.0±0.0	100.0±0.0	100.0±0.0	100.0±0.0	100.0±0.0
	Uniform-C(0.012)			100.0±0.0	100.0±0.0	36.2±0.7	39.6±0.2	100.0±0.0	100.0±0.0	30.9±0.7	37.9±0.2
	CIFAR-10			99.6±0.0	99.6±0.0	7.2±0.2	31.4±0.0	100.0±0.0	100.0±0.0	1.7±0.1	30.8±0.0
	CIFAR-100			99.8±0.0	99.8±0.0	9.5±0.3	31.8±0.1	100.0±0.0	100.0±0.0	2.9±0.2	30.9±0.0
	ImageNet32			100.0±0.0	100.0±0.0	78.1±0.4	85.6±0.3	100.0±0.0	100.0±0.0	83.9±0.4	89.6±0.2
	ImageNet32-C(0.07)			100.0±0.0	100.0±0.0	35.8±0.3	43.5±0.4	100.0±0.0	100.0±0.0	30.2±0.2	40.1±0.5
	SVHN			100.0±0.0	100.0±0.0	78.7±0.3	73.3±0.9	100.0±0.0	100.0±0.0	86.6±0.8	83.3±1.4
	SVHN-C(1.8)			100.0±0.0	100.0±0.0	3.5±0.2	31.0±0.0	100.0±0.0	100.0±0.0	0.5±0.1	30.7±0.0

TABLE 3  
GAD results on GlowGMM trained on FashionMNIST.

Batch size	$m=25$			
	KLODS		Ty-test	
	AUROC	AUPR	AUROC	AUPR
class 0 vs rest	100.0±0.0	100.0±0.0	5.4±1.6	31.2±0.3
class 1 vs rest	100.0±0.0	100.0±0.0	15.7±2.4	33.4±4.9
class 2 vs rest	100.0±0.0	100.0±0.0	0.5±0.5	30.7±0.0
class 3 vs rest	99.9±0.1	99.9±0.1	89.6±2.5	91.3±2.3
class 4 vs rest	100.0±0.0	100.0±0.0	0.7±0.6	30.7±0.0
class 5 vs rest	100.0±0.0	100.0±0.0	64.2±1.4	66.4±2.9
class 6 vs rest	99.9±0.1	99.9±0.1	0.0±0.0	30.7±0.0
class 7 vs rest	100.0±0.0	100.0±0.0	31.4±2.8	46.6±3.3
class 8 vs rest	100.0±0.0	100.0±0.0	0.4±0.5	30.7±0.0
class 9 vs rest	100.0±0.0	100.0±0.0	69.0±3.6	76.0±1.7

fitted Gaussian from OOD representations. See Section D in the supplementary material for more details.

**Mixture of OOD data sets.** We also use the mixture of two data sets as one OOD data set. In such problems, we can treat samples from multiple distributions as from a mixture of distributions. Table 4 shows the results of KLODS when OOD data set is a mixture of two of the three data sets: SVHN, CelebA, and CIFAR-10. We randomly choose 5,000 samples from each data set and get 10,000 samples in total. Our method outperforms the baseline significantly.

**GAD on VAE.** We train convolutional VAE with 8-/16-/32-dimensional latent space on FashionMNIST, SVHN, and CIFAR-10, respectively. The latent space is too small, so we did not split representations and only use KLOD in

experiments. As shown in Table 5, KLOD achieves 98.8%+ AUROC when  $m = 25$  for almost all problems. CIFAR-10 vs CIFAR-100 is also the most difficult problem on VAE. KLOD needs a batch size 150 to achieve 98%+ AUROC. See Table 13 in the supplementary material for details. Nevertheless, KLOD still outperforms Ty-test. Again, Ty-test can be attacked by data manipulations M2. As pointed out by existing work, for vanilla VAE the reconstruction probability is not a reliable criterion for OOD detection [73].

### 5.2.2 PAD Results

We use the SOTA PAD method applicable to flow-based model [70] as the baseline. In [70], the authors modify the official Glow model by using zero padding and removing ActNorm layer. In principle, the baseline method should not be affected by such modification to models. Since the authors did not release their model checkpoint, we reimplement the baseline method using the original Glow model [68]. We also use FLIF [74] as the compressor which is considered as the best compressor in [70]. However, we find that the baseline method did not reach the performance reported in [70]. In [70], the authors did not explain why they modified the official model. We are not aware of why the performance of baseline degenerates on the official Glow model.

**CIFAR-10 vs Others.** Table 6 shows PAD results on CIFAR-10 vs others. Compared with the results reported in [70], our method outperforms the baseline method only on CIFAR-10 vs TinyImageNet. Compared with the reimplementations

TABLE 4

GAD Results of KLODS on Glow with batch size 5 and 10. For SVHN, CIFAR-10, and CelebA, we choose one data set as ID data and the mixture of the other two data sets as OOD data.

ID↓	OOD ↓	Batch size→		$m=5$				$m=10$			
		Method→		KLODS		Ty-test		KLODS		Ty-test	
		Metric→		AUROC	AUPR	AUROC	AUPR	AUROC	AUPR	AUROC	AUPR
SVHN	CelebA+CIFAR-10			100.0±0.0	100.0±0.0	100.0±0.0	100.0±0.0	100.0±0.0	100.0±0.0	100.0±0.0	100.0±0.0
CIFAR-10	SVHN+CelebA			98.2±0.2	98.5±0.2	60.8±0.3	64.4±0.5	99.8±0.0	99.9±0.0	52.8±1.0	58.1±1.1
CelebA	SVHN+CIFAR-10			100.0±0.0	100.0±0.0	20.7±0.2	34.9±0.1	100.0±0.0	100.0±0.0	11.8±0.5	32.3±0.1

TABLE 5  
GAD results of KLOD on VAE.

ID↓	OOD↓	Batch size→		$m=10$				$m=25$			
		Method→		KLOD		Ty-test		KLOD		Ty-test	
		Metric→		AUROC	AUPR	AUROC	AUPR	AUROC	AUPR	AUROC	AUPR
Fash.	MNIST			99.7±0.1	99.5±0.2	100.0±0.0	100.0±0.0	100.0±0.0	100.0±0.0	100.0±0.0	100.0±0.0
	MNIST-C(0.4)			99.8±0.0	99.8±0.0	39.1±0.7	40.5±0.3	100.0±0.0	100.0±0.0	37.6±1.9	39.8±0.7
	notMNIST			100.0±0.0	100.0±0.0	100.0±0.0	100.0±0.0	100.0±0.0	100.0±0.0	100.0±0.0	100.0±0.0
SVHN	CelebA			92.2±0.6	82.3±1.1	100.0±0.0	100.0±0.0	100.0±0.0	100.0±0.0	100.0±0.0	100.0±0.0
	CelebA-C(0.7)			86.2±0.9	76.5±1.5	39.9±1.2	41.2±0.5	100.0±0.0	100.0±0.0	47.4±1.5	44.3±0.7
	CIFAR-10			90.9±1.3	81.3±2.3	100.0±0.0	100.0±0.0	100.0±0.0	100.0±0.0	100.0±0.0	100.0±0.0
	CIFAR-10-C(0.4)			77.6±8.8	69.9±1.3	49.8±0.6	45.8±0.3	99.7±0.2	99.6±0.3	58.8±0.9	50.2±0.4
	CIFAR-100			90.4±0.4	80.3±0.6	100.0±0.0	100.0±0.0	100.0±0.0	100.0±0.0	100.0±0.0	100.0±0.0
	CIFAR-100-C(0.4)			80.5±1.0	73.2±1.8	40.3±0.8	40.7±1.3	99.8±0.0	99.8±0.0	40.5±0.4	41.3±0.2
	Imagenet32			89.3±8.6	80.1±1.5	100.0±0.0	100.0±0.0	100.0±0.0	100.0±0.0	100.0±0.0	100.0±0.0
	Imagenet32-C(0.3)			74.6±0.6	67.8±0.7	27.9±1.0	36.5±0.3	99.0±0.0	99.0±0.0	27.9±1.0	36.5±0.3
ID ↓	OOD ↓	Batch size		$m=25$				$m=50$			
CIFAR-10	CelebA			99.1±0.4	99.1±0.4	100.0±0.0	100.0±0.0	100.0±0.0	100.0±0.0	100.0±0.0	100.0±0.0
	CelebA-C(0.7)			94.2±0.6	93.8±0.8	42.3±1.1	42.8±0.6	100.0±0.0	100.0±0.0	39.3±2.0	41.1±1.0
	Imagenet32			54.0±1.9	53.4±0.7	99.8±0.1	99.8±0.1	94.0±0.6	94.0±0.5	100.0±0.0	100.0±0.0
	Imagenet32-C(0.8)			77.4±1.4	77.3±1.8	47.8±1.5	48.0±1.5	98.8±0.5	98.9±0.4	46.4±1.7	46.8±1.2
	SVHN			91.8±1.5	91.1±2.3	99.8±0.0	99.8±0.0	100.0±0.0	100.0±0.0	100.0±0.0	100.0±0.0
	SVHN-C(1.5)			94.2±1.5	91.1±2.3	60.0±1.7	61.4±1.7	100.0±0.0	100.0±0.0	53.6±2.7	55.7±1.6

mentation on official Glow model, our method outperforms the baseline for most cases.

TABLE 6

PAD results (AUROC) on Glow trained on CIFAR-10.  $S$  [70]: baseline method results reported by [70]. The notation (D) means the method implemented using the model checkpoints released by DeepMind.

OOD	$S$ [70]	$S(D)$	KLODS
Constant	100.0	100.0	98.9
Uniform	100.0	100.0	100.0
CelebA	86.3	62.1	85.2
SVHN	95.0	80.7	82.6
TinyImageNet	71.6	56.3	83.9
CIFAR-100	73.6	50.9	54.1

**SVHN vs Others.** In [70], although the authors claim that the baseline method can detect OOD data with more complexity than ID data (roughly *Category II* problems), they did not evaluate their method on such problems thoroughly. Table 7 shows the results on SVHN vs others. All problems in the top half of Table 7 are *Category II* problems. KLODS can achieve 98.8%+ AUROC and outperforms the baseline. The bottom half of Table 7 shows the results of OOD data with lower contrast (complexity). For these several problems, KLODS is comparable with the baseline.

**CelebA vs others.** We have also conducted experiments on CelebA vs others, which are not evaluated in [70] either. As shown in Table 8, KLODS outperforms the baseline. We notice that KLODS does not always achieve high AUROC in all cases. We think the reason is similar to that for CIFAR-10 vs CIFAR-100. The likelihoods of the train and test split of CelebA do not fit well. This means that  $KL(p_Z||p_Z')$  is not small enough. Unlike on GAD, KLODS on PAD is affected by the possible underfitting or overfitting on CelebA.

TABLE 7

PAD results on Glow trained on SVHN.  $S$ : baseline [70]. We order the problems roughly according to the complexity of OOD data sets. The top four OOD data sets are more complex than SVHN and fall in *Category II*. The rest OOD data sets are simpler than SVHN and fall in *Category I*.

	OOD	$S(D)$		KLODS	
		AUROC	AUPR	AUROC	AUPR
Complex	Uniform	100.0	100.0	100.0	100.0
	ImageNet32	78.7	88.1	99.9	99.9
	CelebA	83.1	86.7	100.0	100.0
	CIFAR-10	43.8	52.7	98.9	99.1
Simple	CIFAR-100	44.9	56.0	98.8	99.9
	CelebA-C(0.08)	81.4	76.7	82.2	80.8
	CIFAR-10-C(0.12)	75.3	70.6	72.5	71.7
	CIFAR-100-C(0.12)	75.2	72.1	75.3	75.3
	Imagenet32-C(0.07)	99.6	99.7	99.8	99.8
	notMNIST	100.0	100.0	99.6	99.7
	Constant	100.0	99.9	99.7	99.3

TABLE 8

PAD results (AUROC) on Glow trained on CelebA.  $S$ : baseline [70].

OOD	$S(D)$		KLODS	
	AUROC	AUPR	AUROC	AUPR
Constant	98.0	92.2	100.0	100.0
Uniform	91.0	82.7	100.0	100.0
ImageNet	16.5	36.0	100.0	100.0
CIFAR-10	55.0	54.3	69.0	67.9
CIFAR-100	53.2	54.8	72.3	71.8
SVHN	83.9	71.8	94.7	95.0

## 6 DISCUSSION

**Normality of representations.** The normality of ID and OOD representation facilitates our theoretical analysis and implementation in OOD detection algorithm on flow-based model. In our experiments, we find that the normality of OOD representation is a widely existing phenomenon under flow-



based model. We observe even representation of random noise has a  $p$ -value greater than 0.05. We are investigating the underlying reason. Most importantly, our method performs even better on *Category II* problems although the criterion computes the lower bound of the KL divergence.

Both Flow-based model and VAE are trained to minimize KL divergence between  $p_Z$  and prior. It seems natural that ID representations should follow Gaussian-like distribution. However, we did not observe such a phenomenon in VAE. In our experiments, we find that not all ID representations in VAE have  $p$ -values greater than 0.05. All OOD representations in VAE do not follow Gaussian-like distribution. We should note that our method on VAE does not have a divergence guarantee as that in flow-based model.

In principle, we can construct latents following any distribution and decode these latents to construct an OOD data set. Such data manipulation can be seen as an attack on the normality of representations. Note that, such manipulation does not make our OOD detection method fail necessarily.

**Limitations.** This work is an attempt to detect OOD data with divergence guarantee for flow-based model. The properties of flow-based model allow us to conduct deeper analysis. Our work has the following three limitations.

The first limitation is that our method requires the model to capture the distribution of training data. Modeling data is a long-standing goal of unsupervised learning [32]. There are two possible solutions to handle CIFAR-10 vs CIFAR-100. The first one is to improve the model. Up to now, we have not tried more advanced flow-based models [75], [76]. We are not aware of any unconditional flow-based model that can model CIFAR-10 satisfactorily. The second possible solution is to use a more sensitive criterion to estimate KL divergence or dependence. For example, our answer 2 to Q1 reminds us to use the sample correlation of representations for GAD. We have tried to use the standard deviation of the set of non-diagonal elements of the correlation matrix as the criterion for GAD. Experimental results show that such criterion achieves 90+% AUROC on CIFAR-10 VS CIFAR-100 with batch size 250, although it needs a larger batch size than KLODS on other problems. We leave this direction as future work.

Besides, when applied to PAD, KLODS sets higher demands on the model. For example, KLODS is affected by the discrepancy of the likelihoods of train and test splits on CelebA vs others.

The second limitation is that PAD performance may decrease when OOD data set has very low contrast (e.g., SVHN vs CelebA-C(0.08)). Nevertheless, our method is still better than the baseline.

Finally, Ty-test applies to flow-based model, VAE, and auto-regressive model. Our method applies to models which learn independent or disentangled representations [50], [51], [52], [77], [78], [79], [80], not including auto-regressive model.

**Models.** We did not conduct more experiments on flow-based models with various architectures as well as other training methods. For VAE, our method is affected by the model architecture and training method. A high-dimensional latent space may contain nearly dead neurons. This may reduce the performance of our method. We did not conduct experiments on other VAE variations, e.g.,  $\beta$ -VAE [80], Factor-VAE [50],  $\beta$ -TCVAE [51], and DIP-VAE [52]. These variations

add more regularization strength on disentanglement and hence have more independent representations than vanilla VAE [53]. We also did not conduct PAD on VAE because the VAE models used in our experiments are small. We have not enough latent variables to split into multiple groups. In the future, we will conduct experiments on larger VAE models and variations.

## 7 RELATED WORK

**OOD Detection.** In [2], Toth *et al.* give a survey on GAD methods and a list of real-world GAD applications. In [3], Chalapathy *et al.* survey a wide range of deep learning-based GAD and PAD methods. In [81], Pang *et al.* also review the deep learning-based anomaly detection methods. According to the availability of supervision information, OOD detection can be classified into three categories: supervised setting, semi-supervised setting, and unsupervised setting. In this paper, we focus on unsupervised OOD detection using flow-based model, so we mainly compare with methods in the same category.

Generally, it seems straightforward to use model likelihood  $p(x)$  (if any) of a generative model to detect OOD data [2], [82]. However, these methods fail when OOD data have higher or similar likelihoods. Choi *et al.* propose using the Watanabe-Akaike Information Criterion (WAIC) to detect OOD data [18]. WAIC penalizes points that are sensitive to the particular choice of posterior model parameters. However, Nalisnick *et al.* [20] point out that WAIC is not stable. Choi *et al.* also propose using typicality test in the latent space to detect OOD data. Our results reported in section 2.2 demonstrate that typicality test in the latent space can be attacked. Sabeti *et al.* propose detecting anomaly based on typicality [83], but their method is not suitable for DGM. Nalisnick *et al.* propose using typicality test on model distribution (Ty-test) for GAD [20]. Ren *et al.* propose to use likelihood ratios for OOD detection [71]. Serrà *et al.* propose using likelihood compensated by input complexity for OOD detection [70]. Before this writing, [20] and [70] are the SOTA GAD and PAD methods applicable to flow-based models under unsupervised setting, respectively. We use them as the baselines in our experiments.

OOD detection can be improved with the help of an auxiliary outlier data set. Schirmmeister *et al.* improve likelihood-ratio-based method by the help of a huge outlier data set (80 Million Tiny Imagenet) [84]. The method in [84] is not purely unsupervised learning due to the exposure to outliers in training as like [58]. Besides, the huge outlier data set includes almost all the image classes in the testing phase. We did not compare with such methods due to different problem settings.

**Theoretical Analysis.** Previous works [26], [85] analyze the training objective of flow-based model in KL divergence form. We apply the property of diffeomorphism to investigate the divergences between distributions in flow-based models for OOD detection. We also propose new theorems on the properties of KL divergence between Gaussians for further analysis. Existing research has explored the upper bound of KL divergence in different settings [86], [87], [88], [89]. To the best of our knowledge, we are not aware of similar work on the properties of KL divergence between

Gaussians. Theorem 2, 3 and 4 can be used as basic theorems in information theory and machine learning fields.

In principle, GMM can approximate a target density better than a single Gaussian [90]. We have tried to use GMM model to estimate  $D_g$  (see Subsection 4.2) but find GMM is worse. We think the reasons are twofold: a) In our problems,  $D_g[pz]$  is Gaussian-like. It is not appropriate to use GMM for ID data. b) The batch size is too small to estimate the parameters of GMM.

**Local pixel dependence.** In [91], Kirichenko *et al.* reshape the representations of flow-based models to original input shape and analyze the induction biases of flow-based model. Their work reveals the reshaped representation manifests local pixel dependence. Our theoretical analysis from the divergence perspective allows strong dependence for OOD data. We also show that the representations with raw shape also manifest local pixel dependence.

**Classification of problems.** We classify OOD problems into *Category I* and *II* according to the variance of data sets. This criterion is roughly similar to the complexity used in [70]. See Figure 30 in the supplementary material for details.

## 8 CONCLUSION

In this paper, we prove theorems to investigate the divergences in flow-based models. Based on these theorems, we answer the question of why cannot sample out OOD data from two perspectives. We observe the normality of ID representations and OOD representations in flow-based model for a wide range of problems. Our theoretical analysis and key observation inspire us to perform GAD by KL divergence. We decompose the KL divergence further to improve our method and support PAD as well. Experimental results demonstrate our method can achieve very strong AUROC for all GAD problems and robust against data manipulations. On the contrary, the SOTA GAD method performs not better than random guessing for challenging problems and can be attacked by data manipulation in almost all cases. For PAD, our method also outperforms the baseline.

## REFERENCES

- [1] V. Chandola, A. Banerjee, and V. Kumar, "Anomaly detection: A survey," *ACM Comput. Surv.*, vol. 41, no. 3, Jul. 2009.
- [2] E. Toth and S. Chawla, "Group deviation detection methods: A survey," *ACM Comput. Surv.*, vol. 51, no. 4, Jul. 2018.
- [3] R. Chalapathy and S. Chawla, "Deep learning for anomaly detection: A survey," 2019.
- [4] K. Muandet and B. Schölkopf, "One-class support measure machines for group anomaly detection," in *Proceedings of the Twenty-Ninth Conference on Uncertainty in Artificial Intelligence*, ser. UAI'13. Arlington, Virginia, USA: AUAI Press, 2013, p. 449–458.
- [5] G. Jorge, C. Stephane, and H. R., "Support measure data description for group anomaly detection," *ODDx3 Workshop on Outlier Definition, Detection, and Description at ACM SIGKDD International Conference on Knowledge Discovery and Data Mining (KDD 2015)*, 2015.
- [6] L. Xiong, B. Poczos, J. Schneider, A. Connolly, and J. VanderPlas, "Hierarchical Probabilistic Models for Group Anomaly Detection," *Journal of Machine Learning Research - Proceedings Track*, vol. 15, pp. 789–797, 2011.
- [7] L. Xiong, B. Póczos, and J. Schneider, "Group anomaly detection using flexible genre models," in *Proceedings of the 24th International Conference on Neural Information Processing Systems*, ser. NIPS'11. Red Hook, NY, USA: Curran Associates Inc., 2011, p. 1071–1079.
- [8] A. Kuppaa, S. Grzonkowski, M. R. Asghar, and N. Le-Khac, "Finding rats in cats: Detecting stealthy attacks using group anomaly detection," in *2019 18th IEEE International Conference On Trust, Security And Privacy In Computing And Communications/13th IEEE International Conference On Big Data Science And Engineering (Trust-Com/BigDataSE)*, 2019, pp. 442–449.
- [9] S. P. Mishra and P. Kumari, "Analysis of Techniques for Credit Card Fraud Detection: A Data Mining Perspective," in *New Paradigm in Decision Science and Management*, S. Patnaik, A. W. H. Ip, M. Tavana, and V. Jain, Eds. Singapore: Springer Singapore, 2020, pp. 89–98.
- [10] Y. Ye, T. Li, D. Adjeroh, and S. S. Iyengar, "A survey on malware detection using data mining techniques," *ACM Comput. Surv.*, vol. 50, no. 3, Jun. 2017.
- [11] D. P. Kingma and P. Dhariwal, "Glow: Generative flow with invertible 1x1 convolutions," in *Advances in Neural Information Processing Systems*, 2018, pp. 10215–10224.
- [12] L. Dinh, J. Sohl-Dickstein, and S. Bengio, "Density estimation using real nvp," in *Proceedings of the International Conference on Learning Representations (ICLR)*, 2017.
- [13] D. P. Kingma and M. Welling, "Auto-encoding variational bayes," in *Proceedings of the International Conference on Learning Representations (ICLR)*, 2014.
- [14] A. Van den Oord, N. Kalchbrenner, L. Espeholt, O. Vinyals, A. Graves *et al.*, "Conditional image generation with pixelcnn decoders," in *Advances in neural information processing systems*, 2016, pp. 4790–4798.
- [15] T. Salimans, A. Karpathy, X. Chen, and D. P. Kingma, "PixelCNN++: Improving the pixelcnn with discretized logistic mixture likelihood and other modifications," *Proceedings of the International Conference on Learning Representations (ICLR)*, 2017.
- [16] E. Nalisnick, A. Matsukawa, Y. W. Teh, D. Gorur, and B. Lakshminarayanan, "Do deep generative models know what they don't know?" *International Conference on Learning Representations (ICLR)*, 2019.
- [17] A. Shafaei, M. Schmidt, and J. J. Little, "Does your model know the digit 6 is not a cat? a less biased evaluation of "outlier" detectors," *arXiv preprint arXiv:1809.04729*, 2018.
- [18] H. Choi and E. Jang, "WAIC, but why?: Generative ensembles for robust anomaly detection," *arXiv preprint arXiv:1810.01392*, 2018.
- [19] V. Škvára, T. Pevný, and V. Šmídl, "Are generative deep models for novelty detection truly better?" *KDD Workshop on Outlier Detection De-Constructed (ODD v5.0)*, 2018.
- [20] E. Nalisnick, A. Matsukawa, Y. W. Teh, and B. Lakshminarayanan, "Detecting out-of-distribution inputs to deep generative models using typicality," *4th workshop on Bayesian Deep Learning (NeurIPS 2019)*, 2019.
- [21] P. Kirichenko, P. Izmailov, and A. Wilson, "Why normalizing flows fail to detect out-of-distribution data," *ArXiv*, vol. abs/2006.08545, 2020.
- [22] E. Fetaya, J. Jacobsen, and R. S. Zemel, "Conditional generative models are not robust," *CoRR*, vol. abs/1906.01171, 2019.
- [23] P. Izmailov, P. Kirichenko, M. Finzi, and A. G. Wilson, "Semi-supervised learning with normalizing flows," 2019.
- [24] K. He, X. Zhang, S. Ren, and J. Sun, "Deep residual learning for image recognition," in *2016 IEEE Conference on Computer Vision and Pattern Recognition (CVPR)*. Los Alamitos, CA, USA: IEEE Computer Society, jun 2016, pp. 770–778.
- [25] L. Dinh, D. Krueger, and Y. Bengio, "NICE: Non-linear independent components estimation," *arXiv preprint arXiv:1410.8516*, 2014.
- [26] G. Papamakarios, E. Nalisnick, D. J. Rezende, S. Mohamed, and B. Lakshminarayanan, "Normalizing flows for probabilistic modeling and inference," 2019.
- [27] R. Vershynin, *High-dimensional probability: An introduction with applications in data science*. Cambridge University Press, 2018, vol. 47.
- [28] T. M. Cover and J. A. Thomas, *Elements of information theory*. John Wiley & Sons, 2012.
- [29] L. Pardo, *Statistical Inference Based on Divergence Measures*. New York: Chapman and Hall/CRC, 2006.
- [30] F. Nielsen, "An elementary introduction to information geometry," *arXiv preprint arXiv:1808.08271*, 2018.
- [31] L. E. J. Brouwer, "Beweis der invarianz des n-dimensionalen gebiets," *Mathematische Annalen*, vol. 71, no. 3, pp. 305–313, 1911.
- [32] C. M. Bishop, *Pattern Recognition and Machine Learning (Information Science and Statistics)*. Berlin, Heidelberg: Springer-Verlag, 2006.

- [33] J. H. Lambert, "Observationes variae in mathesin puram," *Acta Helveticae physico-mathematico-anatomico-botanico-medica*, Band III, pp. 128–168, 1758.
- [34] R. M. Corless, G. H. Gonnet, D. E. Hare, D. J. Jeffrey, and D. E. Knuth, "On the Lambert W function," *Advances in Computational Mathematics*, vol. 5, no. 1, pp. 329–359, 1996.
- [35] Y. Zhang, W. Liu, Z. Chen, K. Li, and J. Wang, "On the properties of Kullback-Leibler divergence between gaussians," *arXiv preprint arXiv:2102.05485*, 2021.
- [36] N. Mohd Razali and B. Yap, "Power comparisons of shapiro-wilk, kolmogorov-smirnov, lilliefors and anderson-darling tests," *J. Stat. Model. Analytics*, vol. 2, 01 2011.
- [37] M. Giraudo, L. Sacerdote, and R. Sirovich, "Non-parametric estimation of mutual information through the entropy of the linkage," *Entropy*, vol. 15, no. 12, p. 5154–5177, Nov 2013.
- [38] J. L. Rodgers and W. A. Nicewander, "Thirteen ways to look at the correlation coefficient," *The American Statistician*, vol. 42, no. 1, pp. 59–66, 1988.
- [39] H. Hoijtink, I. Klugkist, L. D. Broemeling, R. Jensen, Q. Shen, S. Mukherjee, R. A. Bailey, J. L. Rosenberger, J. D. Leeuw, E. Meijer, B. G. Leroux, A. B. Tsybakov, W. Wefelmeyer, P. C. Consul, F. Famoye, and D. Richards, "Introduction to nonparametric estimation," 2009.
- [40] X. Nguyen, M. J. Wainwright, and M. I. Jordan, "Estimating divergence functionals and the likelihood ratio by penalized convex risk minimization," in *In Advances in Neural Information Processing Systems (NIPS)*, 2007.
- [41] P. K. Rubenstein, O. Bousquet, J. Djolonga, C. Riquelme, and I. O. Tolstikhin, "Practical and consistent estimation of f-divergences," *Annual Conference on Neural Information Processing Systems*, vol. abs/1905.11112, pp. 4072–4082, 2019.
- [42] Qing Wang, S. R. Kulkarni, and S. Verdu, "Divergence estimation of continuous distributions based on data-dependent partitions," *IEEE Transactions on Information Theory*, vol. 51, no. 9, pp. 3064–3074, 2005.
- [43] Q. Wang, S. R. Kulkarni, and S. Verdu, "Divergence estimation for multidimensional densities via  $k$ -nearest-neighbor distances," *IEEE Transactions on Information Theory*, vol. 55, no. 5, pp. 2392–2405, 2009.
- [44] X. Nguyen, M. J. Wainwright, and M. I. Jordan, "Estimating divergence functionals and the likelihood ratio by convex risk minimization," *IEEE Trans. Inf. Theor.*, vol. 56, no. 11, p. 5847–5861, Nov. 2010.
- [45] K. R. Moon and A. O. Hero, "Ensemble estimation of multivariate f-divergence," in *2014 IEEE International Symposium on Information Theory*, 2014, pp. 356–360.
- [46] A. Gambardella, A. G. Baydin, and P. H. S. Torr, "Transflow learning: Repurposing flow models without retraining," 2019.
- [47] E. Gonzalez-Estrada and J. A. Villasenor-Alva, "mvshapitertest: Generalized shapiro-wilk test for multivariate normality," 2013, r package version 1.0.
- [48] L. Pardo, *Statistical inference based on divergence measures*. CRC press, 2018.
- [49] C. P. Burgess, I. Higgins, A. Pal, L. Matthey, N. Watters, G. Desjardins, and A. Lerchner, "Understanding disentangling in  $\beta$ -vae," in *Workshop on Learning Disentangled Representations at the 31st Conference on Neural Information Processing Systems*, 2018.
- [50] H. Kim and A. Mnih, "Disentangling by factorising," in *Proceedings of the 35th International Conference on Machine Learning*, ser. Proceedings of Machine Learning Research, J. Dy and A. Krause, Eds., vol. 80. Stockholm: Stockholm Sweden: PMLR, 10–15 Jul 2018, pp. 2649–2658.
- [51] T. Q. Chen, X. Li, R. B. Grosse, and D. K. Duvenaud, "Isolating sources of disentanglement in variational autoencoders," in *Advances in Neural Information Processing Systems 31*, S. Bengio, H. Wallach, H. Larochelle, K. Grauman, N. Cesa-Bianchi, and R. Garnett, Eds. Curran Associates, Inc., 2018, pp. 2610–2620.
- [52] A. Kumar, P. Sattigeri, and A. Balakrishnan, "Variational inference of disentangled latent concepts from unlabeled observations," in *International Conference on Learning Representations*, 2017.
- [53] F. Locatello, S. Bauer, M. Lucic, G. Rätsch, S. Gelly, B. Schölkopf, and O. Bachem, "Challenging common assumptions in the unsupervised learning of disentangled representations," in *Proceedings of the 36th International Conference on Machine Learning*, 2019.
- [54] M. D. Hoffman and M. J. Johnson, "ELBO surgery: yet another way to carve up the variational evidence lower bound," in *Workshop in Advances in Approximate Bayesian Inference, NIPS*, vol. 1, 2016.
- [55] T. Salimans, A. Karpathy, X. Chen, and D. P. Kingma, "Pixelcnn++: A pixelcnn implementation with discretized logistic mixture likelihood and other modifications," in *ICLR*, 2017.
- [56] K. Lee, K. Lee, H. Lee, and J. Shin, "A simple unified framework for detecting out-of-distribution samples and adversarial attacks," in *Advances in Neural Information Processing Systems*, 2018, pp. 7167–7177.
- [57] D. Hendrycks and K. Gimpel, "A baseline for detecting misclassified and out-of-distribution examples in neural networks," in *Proceedings of the International Conference on Learning Representations (ICLR)*, 2017.
- [58] D. Hendrycks, M. Mazeika, and T. G. Dietterich, "Deep anomaly detection with outlier exposure," *International Conference on Learning Representations (ICLR)*, 2019.
- [59] Y. LeCun, L. Bottou, Y. Bengio, P. Haffner et al., "Gradient-based learning applied to document recognition," *Proceedings of the IEEE*, vol. 86, no. 11, pp. 2278–2324, 1998.
- [60] H. Xiao, K. Rasul, and R. Vollgraf, "Fashion-MNIST: a novel image dataset for benchmarking machine learning algorithms," 2017.
- [61] Y. Bulatov, "notMNIST," <http://yaroslavvb.blogspot.com/2011/09/notmnist-dataset.html>, 2011, accessed October 4, 2019.
- [62] A. Krizhevsky, G. Hinton et al., "Learning multiple layers of features from tiny images," Citeseer, Tech. Rep., 2009.
- [63] Y. Netzer, T. Wang, A. Coates, A. Bissacco, B. Wu, and A. Y. Ng, "Reading digits in natural images with unsupervised feature learning," 2011.
- [64] Z. Liu, P. Luo, X. Wang, and X. Tang, "Deep learning face attributes in the wild," in *Proceedings of International Conference on Computer Vision (ICCV)*, December 2015.
- [65] Stanford, <https://tiny-imagenet.herokuapp.com/>.
- [66] J. Deng, W. Dong, R. Socher, L.-J. Li, K. Li, and L. Fei-Fei, "ImageNet: A Large-Scale Hierarchical Image Database," in *CVPR09*, 2009.
- [67] OpenAI, "Glow," <https://github.com/openai/glow>, 2018.
- [68] DeepMind, <https://github.com/y0ast/Glow-PyTorch>.
- [69] M. Buckland and F. Gey, "The relationship between recall and precision," *Journal of the American society for information science*, vol. 45, no. 1, pp. 12–19, 1994.
- [70] J. Serrà, D. Álvarez, V. Gómez, O. Slizovskaia, J. F. Núñez, and J. Luque, "Input complexity and out-of-distribution detection with likelihood-based generative models," in *International Conference on Learning Representations*, 2020.
- [71] J. Ren, P. J. Liu, E. Fertig, J. Snoek, R. Poplin, M. A. DePristo, J. V. Dillon, and B. Lakshminarayanan, "Likelihood ratios for out-of-distribution detection," 2019.
- [72] A. Atanov, A. Volokhova, A. Ashukha, I. Sosnovik, and D. Vetrov, "Semi-conditional normalizing flows for semi-supervised learning," 2019.
- [73] J. An and S. Cho, "Variational autoencoder based anomaly detection using reconstruction probability," *Special Lecture on IE*, vol. 2, no. 1, 2015.
- [74] J. Sneyers and P. Wuille, "FLIF: Free lossless image format based on maniac compression," in *2016 IEEE International Conference on Image Processing (ICIP)*, 2016, pp. 66–70.
- [75] J. Ho, X. Chen, A. Srinivas, Y. Duan, and P. Abbeel, "Flow++: Improving flow-based generative models with variational dequantization and architecture design," in *Proceedings of the 36th International Conference on Machine Learning*, K. Chaudhuri and R. Salakhutdinov, Eds., vol. 97. Long Beach, California, USA: PMLR, 09–15 Jun 2019, pp. 2722–2730.
- [76] J. Behrmann, W. Grathwohl, R. T. Q. Chen, D. Duvenaud, and J.-H. Jacobsen, "Invertible residual networks," in *Proceedings of the 36th International Conference on Machine Learning*, ser. Proceedings of Machine Learning Research, K. Chaudhuri and R. Salakhutdinov, Eds., vol. 97. Long Beach, California, USA: PMLR, 09–15 Jun 2019, pp. 573–582.
- [77] N. . D. Challenge, <https://www.aicrowd.com/challenges/neurips-2019-disentanglement-challenge>.
- [78] I. Higgins, D. Amos, D. Pfau, S. Racaniere, L. Matthey, D. Rezende, and A. Lerchner, "Towards a definition of disentangled representations," 2018.
- [79] C. Eastwood and C. K. I. Williams, "A framework for the quantitative evaluation of disentangled representations," in *International Conference on Learning Representations*, 2018.
- [80] I. Higgins, L. Matthey, A. Pal, C. Burgess, X. Glorot, M. Botvinick, S. Mohamed, and A. Lerchner, "beta-vae: Learning basic visual concepts with a constrained variational framework," *ICLR*, vol. 2, no. 5, p. 6, 2017.

- [81] G. Pang, C. Shen, L. Cao, and A. V. D. Hengel, "Deep learning for anomaly detection: A review," *ACM Comput. Surv.*, vol. 54, no. 2, Mar. 2021. [Online]. Available: <https://doi.org/10.1145/3439950>
- [82] M. A. F. Pimentel, D. A. Clifton, C. Lei, and L. Tarassenko, "A review of novelty detection," *Signal Processing*, vol. 99, no. 6, pp. 215–249, 2014.
- [83] E. Sabeti and A. Hostmadsen, "Data discovery and anomaly detection using atypicality for real-valued data," *Entropy*, vol. 21, no. 3, p. 219, 2019.
- [84] R. T. Schirrmeyer, Y. Zhou, T. Ball, and D. Zhang, "Understanding Anomaly Detection with DeepInvertible Networks through Hierarchies of Distributions and Features," in *Advances in Neural Information Processing Systems* 33. Curran Associates, Inc., 2020.
- [85] G. Papamakarios, T. Pavlakou, and I. Murray, "Masked Autoregressive Flow for Density Estimation," in *Advances in Neural Information Processing Systems* 30. Curran Associates, Inc., 2017, pp. 2338–2347.
- [86] A. Sayyareh, "A New Upper Bound for Kullback-Leibler Divergence," *Applied Mathematical Sciences*, vol. 5, pp. 3303–3317, 2011.
- [87] J. . Durrieu, J. . Thiran, and F. Kelly, "Lower and upper bounds for approximation of the kullback-leibler divergence between gaussian mixture models," in *2012 IEEE International Conference on Acoustics, Speech and Signal Processing (ICASSP)*, 2012, pp. 4833–4836.
- [88] F. Nielsen and K. Sun, "Guaranteed bounds on the kullback-leibler divergence of univariate mixtures," *IEEE Signal Processing Letters*, vol. 23, no. 11, pp. 1543–1546, 2016.
- [89] H. Li, J. Han, T. Zheng, and G. Zheng, "Upper and lower bounds for approximation of the kullback-leibler divergence between hidden markov models," in *2013 IEEE International Conference on Acoustics, Speech and Signal Processing*, 2013, pp. 7609–7613.
- [90] S. Stergiopoulos, *Advanced Signal Processing Handbook*. CRC Press, 2001.
- [91] P. Kirichenko, P. Izmailov, and A. G. Wilson, "Why normalizing flows fail to detect out-of-distribution data," *ICML workshop on Invertible Neural Networks and Normalizing Flows*, 2020 (NeurIPS 2020), 2020.
- [92] S. M. Ali and S. D. Silvey, "A general class of coefficients of divergence of one distribution from another," *Journal of the Royal Statistical Society: Series B (Methodological)*, vol. 28, no. 1, pp. 131–142, 1966.
- [93] M. L. Menéndez, D. Morales, L. Pardo, and M. Salicrú, "Asymptotic behaviour and statistical applications of divergence measures in multinomial populations: a unified study," *Statistical Papers*, vol. 36, no. 1, pp. 1–29, 1995.

## APPENDIX A DIVERGENCE

In our theorem, we use  $\phi$ -divergence (also called  $f$ -divergence) defined by:

**Definition 2 ( $\phi$ -divergence)** The  $\phi$ -divergence between two densities  $p(x)$  and  $q(x)$  is defined by

$$D_\phi(p, q) = \int \phi(p(x)/q(x))q(x)dx, \quad (17)$$

where  $\phi$  is a convex function on  $[0, \infty)$  such that  $\phi(1) = 0$ . When  $q(x) = 0$ ,  $0\phi(0/0) = 0$  and  $0\phi(p/0) = \lim_{t \rightarrow \infty} \phi(t)/t$  [92].

$\phi$ -divergence family is used widely in machine learning fields. As shown in Table 9, many commonly used measures including the KL divergence, Jensen-Shannon divergence, and squared Hellinger distance belong to  $\phi$ -divergence family. Many  $\phi$ -divergences are not proper distance metrics and do not satisfy the triangle inequality.

We also use  $(h, \phi)$ -divergence defined by:

**Definition 3 ( $(h, \phi)$ -divergence)** The  $(h, \phi)$ -divergence between two densities  $p(x)$  and  $q(x)$  is defined by

$$D_\phi^h(p, q) = h(D_\phi(p, q)), \quad (18)$$

where  $h$  is a differentiable increasing real function from  $[0, \phi(0) + \lim_{t \rightarrow \infty} \phi(t)/t]$  onto  $[0, \infty)$  [93].

TABLE 9  
Examples of  $\phi$ -divergence family

$\phi(x)$	Divergence
$x \log x - x + 1$	Kullback-Leibler
$-\log x + x - 1$	Minimum Discrimination Information
$(x - 1) \log x$	$J$ -Divergence
$\frac{1}{2} 1 - x $	Total Variation Distance
$(1 - \sqrt{x})^2$	Squared Hellinger distance
$x \log \frac{2x}{x+1} + \log \frac{2}{x+1}$	Jensen-Shannon divergence

$(h, \phi)$ -divergence includes a broader range of divergences than  $\phi$ -divergence. For example, Rényi distance belongs to  $(h, \phi)$ -divergence family.

## APPENDIX B TABLES

TABLE 10  
Some approximate values of the supremum of KL divergence

$\varepsilon$	0.001	0.005	0.01	0.05	0.1	0.5
sup	0.001	0.006	0.011	0.069	0.016	1.732

## APPENDIX C MODEL DETAILS

We use both DeepMind and OpenAI's official implementations of Glow model. The model consists of three stages, each of which contains 32 coupling layers with width 512. After each stage, the latent variables are split into two parts, one half is treated as the final representations and another half is processed by the next stage. In our experiments, we use only the output of the last stage with shape (4,4,48) as representation. We use additive coupling layers for grayscale data sets and CelebA and use affine coupling layers for SVHN and CIFAR-10. We find no difference between these two coupling layers for OOD detection. All priors are standard Gaussian except for CIFAR-10, which has learned mean and diagonal covariance. All models are trained using Adamax optimization method with a batch size of 64. The learning rate is increased from 0 up to 0.001 in the first 10 epochs and keeps invariable in remaining epochs. Flow-based models are very resource consuming. We train Glow on FashionMNIST/SVHN/CelebA32 for 130/390/2000 epochs respectively. For fairness, we use the checkpoint released by DeepMind [68] for CIFAR-10. We have also conducted experiments using the checkpoints released by OpenAI [67] for CIFAR-10 vs others. The results are similar.

For VAE, we use convolutional architecture in the encoder and decoder. The encoder consists three  $4 \times 4 \times 64$  convolution layers. On top of convolutional layers, two dense layer heads output the mean  $\mu(x)$  and the standard variance  $\sigma(x)$  respectively. The decoder has the mirrored architecture as encoder. All activations are LeakyReLU with  $\alpha = 0.3$ . For FashionMNIST, SVHN, and CIFAR-10, we use 8-, 16- and 32-dimensional latent space respectively. Models are trained



TABLE 11  
GAD Results of KLODS on Glow with batch sizes 2 and 4.

ID↓	OOD↓	Batch size →		$m=2$				$m=4$			
		Method→	Metric→	KLODS		Ty-test		KLODS		Ty-test	
				AUROC	AUPR	AUROC	AUPR	AUROC	AUPR	AUROC	AUPR
Fash.	Constant			100.0±0.0	100.0±0.0	40.6±0.4	41.3±0.2	100.0±0.0	100.0±0.0	41.0±0.5	41.6±0.2
	MNIST			91.6±0.1	91.8±0.2	88.7±0.2	81.1±0.4	99.4±0.0	99.4±0.0	96.1±0.1	93.2±0.1
	MNIST-C(10.0)			97.2±0.1	97.3±0.1	74.0±0.3	65.2±0.2	100.0±0.0	100.0±0.0	85.4±0.2	77.4±0.5
	notMNIST			99.2±0.0	99.4±0.0	64.0±0.3	61.8±0.3	100.0±0.0	100.0±0.0	74.3±0.4	71.2±0.3
	notMNIST-C(0.005)			100.0±0.0	100.0±0.0	23.2±0.2	35.3±0.0	100.0±0.0	100.0±0.0	24.8±0.3	35.7±0.1
SVHN	Constant			100.0±0.0	100.0±0.0	100.0±0.0	100.0±0.0	100.0±0.0	100.0±0.0	100.0±0.0	100.0±0.0
	Uniform			100.0±0.0	100.0±0.0	100.0±0.0	100.0±0.0	100.0±0.0	100.0±0.0	100.0±0.0	100.0±0.0
	Uniform-C(0.008)			100.0±0.0	100.0±0.0	14.9±0.1	33.3±0.0	100.0±0.0	100.0±0.0	14.2±0.5	33.2±0.1
	CelebA			99.9±0.0	99.9±0.0	100.0±0.0	100.0±0.0	100.0±0.0	100.0±0.0	100.0±0.0	100.0±0.0
	CelebA-C(0.08)			96.3±0.1	96.6±0.1	44.1±0.3	43.7±0.2	99.3±0.0	99.3±0.0	49.2±0.3	46.2±0.1
	CIFAR-10			99.0±0.1	99.1±0.0	99.9±0.0	99.9±0.0	99.9±0.0	99.9±0.0	100.0±0.0	100.0±0.0
	CIFAR-10-C(0.12)			92.1±0.2	92.9±0.1	37.5±0.2	40.4±0.1	95.9±0.1	96.4±0.1	33.7±0.4	38.6±0.2
	CIFAR-100			98.9±0.1	99.1±0.1	99.9±0.0	99.9±0.0	99.9±0.0	99.9±0.0	100.0±0.0	100.0±0.0
	CIFAR-100-C(0.12)			92.3±0.1	93.1±0.1	41.1±0.3	42.4±0.1	95.7±0.2	96.2±0.2	37.4±0.2	40.4±0.1
	ImageNet32			100.0±0.0	100.0±0.0	100.0±0.0	100.0±0.0	100.0±0.0	100.0±0.0	100.0±0.0	100.0±0.0
CIFAR-10	ImageNet32-C(0.07)			97.8±0.1	98.1±0.1	48.4±0.3	48.2±0.1	100.0±0.0	100.0±0.0	42.5±0.3	44.1±0.1
	Constant			100.0±0.0	100.0±0.0	100.0±0.0	100.0±0.0	100.0±0.0	100.0±0.0	100.0±0.0	100.0±0.0
	Uniform			100.0±0.0	100.0±0.0	100.0±0.0	100.0±0.0	100.0±0.0	100.0±0.0	100.0±0.0	100.0±0.0
	Uniform-C(0.02)			100.0±0.0	100.0±0.0	9.9±0.0	32.5±0.0	100.0±0.0	100.0±0.0	11.2±0.0	32.8±0.0
	CelebA			93.3±0.1	94.6±0.1	98.0±0.1	98.1±0.0	98.4±0.1	98.7±0.1	99.9±0.0	99.9±0.0
	CelebA-C(0.3)			72.4±0.3	71.6±0.3	32.4±0.3	38.1±0.1	81.3±0.3	81.2±0.3	29.7±0.4	37.1±0.1
	ImageNet32			82.2±0.2	85.2±0.1	93.1±0.2	94.6±0.2	87.8±0.2	90.2±0.2	98.3±0.2	98.7±0.1
	ImageNet32-C(0.3)			68.2±0.1	69.1±0.3	47.8±0.3	48.0±0.2	70.2±0.3	71.0±0.2	42.6±0.9	44.0±0.6
	SVHN			90.0±0.1	90.7±0.2	91.2±0.1	88.1±0.3	96.2±0.1	96.5±0.1	97.6±0.1	96.8±0.2
	SVHN-C(2.0)			99.1±0.1	99.2±0.0	39.2±0.1	64.0±0.1	100.0±0.0	100.0±0.0	35.2±0.5	61.9±0.2
CelebA	Constant			100.0±0.0	100.0±0.0	100.0±0.0	100.0±0.0	100.0±0.0	100.0±0.0	100.0±0.0	100.0±0.0
	Uniform			100.0±0.0	100.0±0.0	100.0±0.0	100.0±0.0	100.0±0.0	100.0±0.0	100.0±0.0	100.0±0.0
	Uniform-C(0.12)			99.2±0.0	99.3±0.0	35.1±0.2	39.3±0.1	100.0±0.0	100.0±0.0	29.4±0.4	37.5±0.1
	CIFAR-10			86.3±0.2	86.4±0.2	21.4±0.2	34.6±0.1	98.5±0.1	98.6±0.1	10.2±0.3	31.9±0.1
	CIFAR-100			89.6±0.2	90.0±0.2	25.0±0.2	35.9±0.0	99.2±0.1	99.3±0.1	12.9±0.1	32.5±0.0
	ImageNet32			100.0±0.0	100.0±0.0	76.4±0.3	83.5±0.1	100.0±0.0	100.0±0.0	76.9±0.4	84.5±0.2
	ImageNet32-C(0.07)			97.5±0.1	97.7±0.0	43.2±0.1	48.4±0.2	100.0±0.0	100.0±0.0	37.9±0.2	45.0±0.2
	SVHN			99.9±0.0	99.9±0.0	69.3±0.1	62.5±0.1	100.0±0.0	100.0±0.0	76.0±0.2	70.5±0.4
	SVHN-C(1.8)			100.0±0.0	100.0±0.0	14.5±0.2	32.9±0.1	100.0±0.0	100.0±0.0	5.6±0.2	31.3±0.0

using Adam without dropout. The learning rate is  $5 \times 10^{-4}$  with no decay.

## APPENDIX D MORE EXPERIMENTAL RESULTS

### D.1 GAD Results on Glow

**KLODS.** Table 11 shows GAD results of KLODS with batch size 2 and 4.

**GlowGMM.** Table 12 shows the results of using  $p(\mathbf{z})$  for 1 vs rest classification on FashionMNIST with GlowGMM.  $p(\mathbf{z})$  is a bad criterion for OOD detection.

Figure 6(a) shows the generated images using noise sampled from the Gaussian components  $\mathcal{N}_i(\boldsymbol{\mu}_i, \text{diag}(\boldsymbol{\sigma}_i^2))$  as prior. The  $i$ -th column corresponds to the  $i$ -th Gaussian  $\mathcal{N}_i$ . Figure 6(b) shows the generated images using the similar operation in Section 4.1.1. For each  $i$ , we compute the representations of the  $((i+1)\%10)$ -th class and normalize them under  $\mathcal{N}_i(\boldsymbol{\mu}_i, \text{diag}(\boldsymbol{\sigma}_i^2))$  as  $\mathbf{z}' = (\mathbf{z} - \boldsymbol{\mu}_i)/\boldsymbol{\sigma}_i$ . We use the normalized representation to fit a Gaussian  $\tilde{\mathcal{N}}_i(\tilde{\boldsymbol{\mu}}_{i'}, \tilde{\boldsymbol{\Sigma}}_{i'})$ . Then we sample  $\epsilon_{i'} \sim \tilde{\mathcal{N}}_i(\tilde{\boldsymbol{\mu}}_{i'}, \tilde{\boldsymbol{\Sigma}}_{i'})$ , and compute  $f^{-1}(\epsilon_{i'} \cdot \boldsymbol{\sigma}_i + \boldsymbol{\mu}_i)$  to generate new images. As shown in Figure 6(b), we can generate almost high quality images of the  $((i+1)\%10)$ -th class from the fitted Gaussian.

In Section 1 we have shown that the centroids of components are close to each other. The results shown in Figure 6(b) show that correlation of representation is more critical than the norm in GlowGMM.

### D.2 GAD Results on VAE

Table 13 shows the GAD results on convolutional VAE trained on CIFAR10 vs CIFAR100/ImageNet32.

Table 14 shows the results of using reconstruction probability  $E_{\mathbf{z} \sim q_\phi}[\log p_\theta(\mathbf{x}|\mathbf{z})]$  for OOD detection in VAE.

## APPENDIX E FIGURES

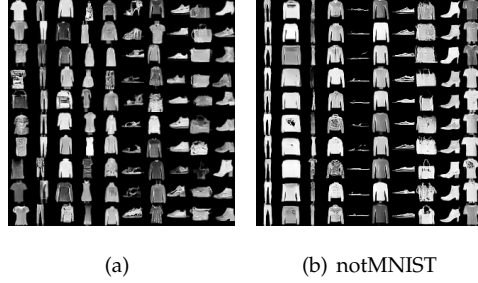


Fig. 6. GlowGMM with 10 components trained on FashionMNIST. (a) sampling from  $\mathcal{N}_i(\mu_i, \text{diag}(\sigma_i^2))$ . The  $i$ -th column corresponds to Gaussian  $\mathcal{N}_i$ . (b) For the  $i$ -th Gaussian  $\mathcal{N}_i$ , we fit another Gaussian  $\tilde{\mathcal{N}}_i(\tilde{\mu}_{i'}, \tilde{\Sigma}_{i'})$  using the normalized representations (by parameters of  $\mathcal{N}_i$ ) of inputs of the  $((i+1)\%10)$ -th class. The  $i$ -th column shows images generated from  $\tilde{\mathcal{N}}_i$ .

TABLE 12  
GlowGMM trained on FashionMNIST. Use  $p(z)$  as criterion for 1 vs rest classification.

Method	$p(z)$	
	AUROC	AUPR
class 0 vs rest	72.7±1.6	72.0±1.4
class 1 vs rest	85.1±0.6	86.2±0.6
class 2 vs rest	74.8±4.5	76.9±4.0
class 3 vs rest	68.9±4.7	71.2±4.5
class 4 vs rest	77.1±2.1	78.4±3.2
class 5 vs rest	71.7±1.4	71.9±1.2
class 6 vs rest	73.5±7.8	73.7±8.6
class 7 vs rest	86.9±0.4	88.6±0.4
class 8 vs rest	55.5±0.9	53.8±0.5
class 9 vs rest	86.6±0.3	87.1±0.3

TABLE 13  
VAE trained on CIFAR10 and tested on CIFAR100. Each row is for one batch size.

Problem	CIFAR10 vs CIFAR100				CIFAR10 vs Imagenet32			
	KLOD		Ty-test		KLOD		Ty-test	
Metric	AUROC	AUPR	AUROC	AUPR	AUROC	AUPR	AUROC	AUPR
$m=50$	72.9±0.7	73.7±2.1	<b>73.8±0.5</b>	<b>74.3±1.8</b>	94.0±0.6	94.0±0.5	<b>100.0±0.0</b>	<b>100.0±0.0</b>
$m=100$	<b>90.9±1.0</b>	<b>91.3±1.3</b>	82.6±0.5	83.5±1.1	99.9±0.2	99.9±0.2	<b>100.0±0.0</b>	<b>100.0±0.0</b>
$m=150$	<b>98.0±0.4</b>	<b>98.1±0.5</b>	88.4±1.3	88.6±2.3	<b>100.0±0.0</b>	<b>100.0±0.0</b>	<b>100.0±0.0</b>	<b>100.0±0.0</b>

TABLE 14  
VAE trained on CIFAR10. Use reconstruction probability for OOD data detection.

Method	reconstruction probability	
	AUROC	AUPR
SVHN	17.6±0.0	34.3±0.0
CelebA	83.1±0.0	82.5±0.0
Imagenet32	72.4±0.2	75.0±0.1
CIFAR100	52.3±0.0	53.6±0.0

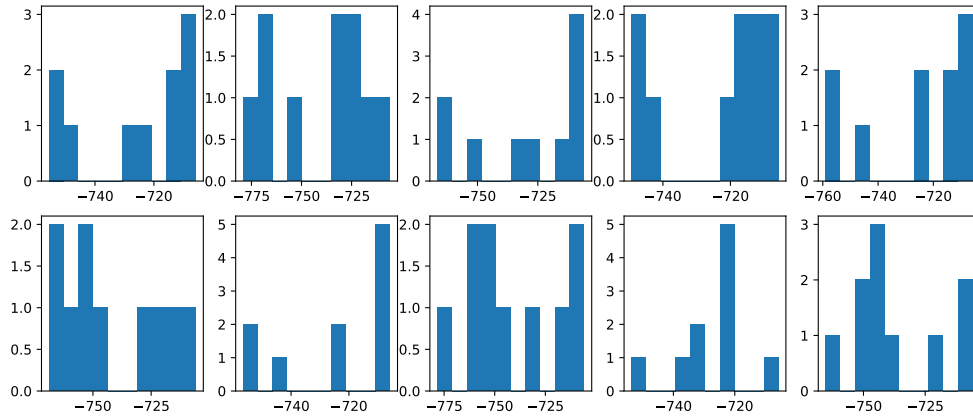


Fig. 7. Train GlowGMM on FashionMNIST. The  $i$ -th subfigure shows the histogram of log-probabilities of 10 centroids under the  $i$ -th Gaussian component. All log-probabilities are close to  $768 \times \log(1/\sqrt{2\pi}) \approx -705.74$ , which is the log-probability of the center of 768-dimensional standard Gaussian. These results indicate these centroids are close to each others.

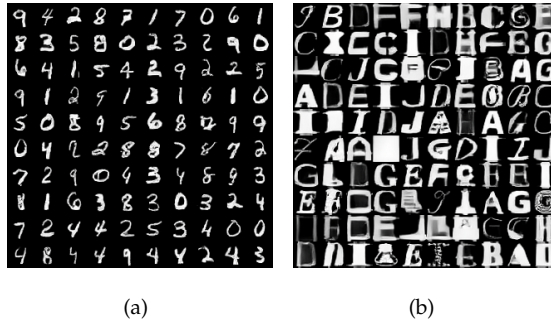


Fig. 8. Train Glow on FashionMNIST and test on MNIST and notMNIST. We scale the representations of OOD dataset to the typical set of prior Gaussian. The scaled latent vectors still corresponds to clear (a) hand-written digits or (b) letters.

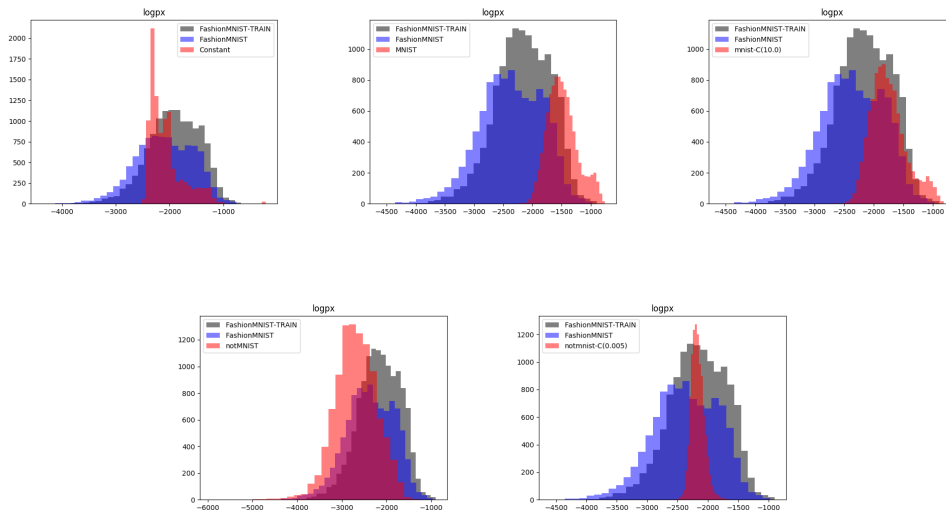


Fig. 9. Glow trained on FashionMNIST. Histogram of  $\log p(x)$ . We can manipulate the likelihood distribution of OOD dataset by adjusting the contrast. “ $C(k)$ ” means the dataset with adjusted contrast by a factor of  $k$ .

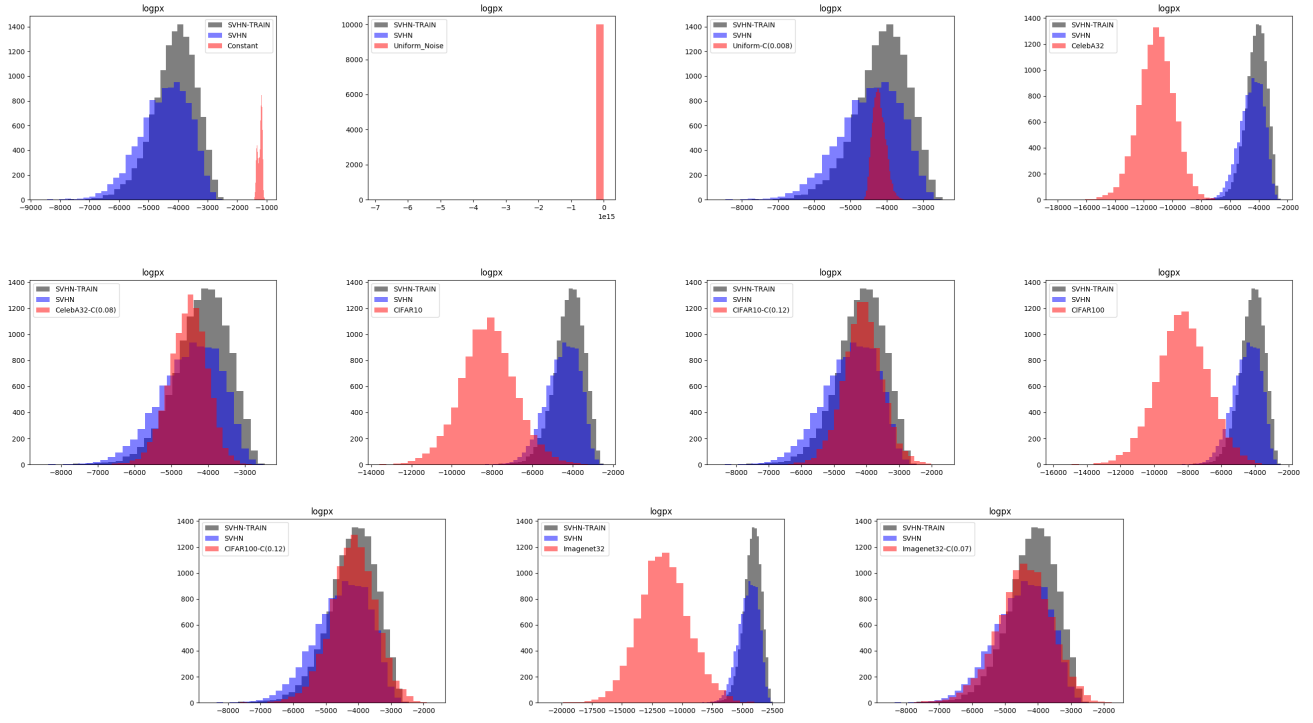


Fig. 10. Glow trained on SVHN. Histogram of  $\log p(\mathbf{x})$ . We can manipulate the likelihood distribution of OOD dataset by adjusting the contrast. “-C( $k$ )” means the dataset with adjusted contrast by a factor of  $k$ .

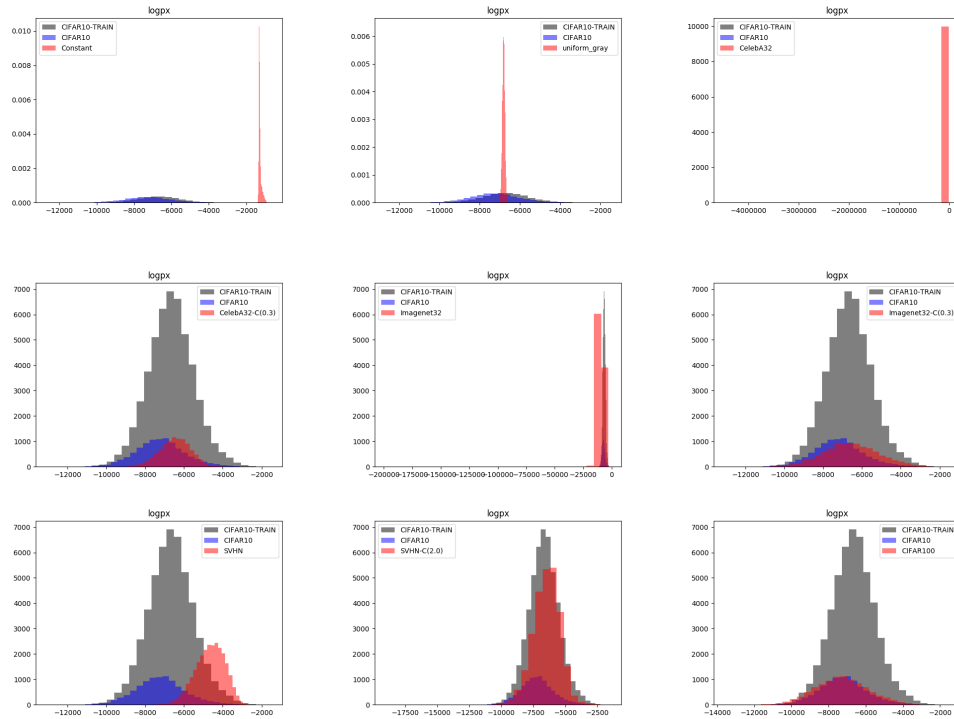


Fig. 11. Glow trained on CIFAR10. Histogram of  $\log p(\mathbf{x})$ . We can manipulate the likelihood distribution of OOD dataset by adjusting the contrast. “-C( $k$ )” means the dataset with adjusted contrast by a factor of  $k$ . For CIFAR10 vs CelebA, the range of  $\log p(\mathbf{x})$  of CelebA is too large. For CIFAR10 vs Uniform,  $\log p(\mathbf{x})$  of Uniform are too small.



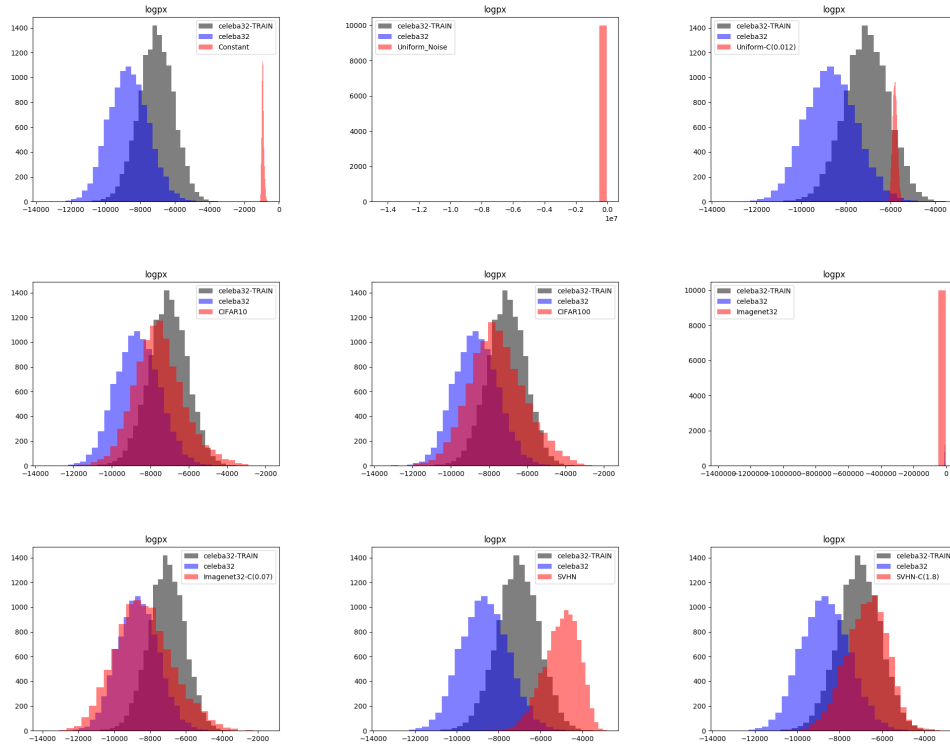


Fig. 12. Glow trained on CelebA. Histogram of  $\log p(x)$ . We can manipulate the likelihood distribution of OOD dataset by adjusting the contrast. “ $-C(k)$ ” means the dataset with adjusted contrast by a factor of  $k$ . It is hard to make the likelihoods of train and test split fit well on the official Glow model.

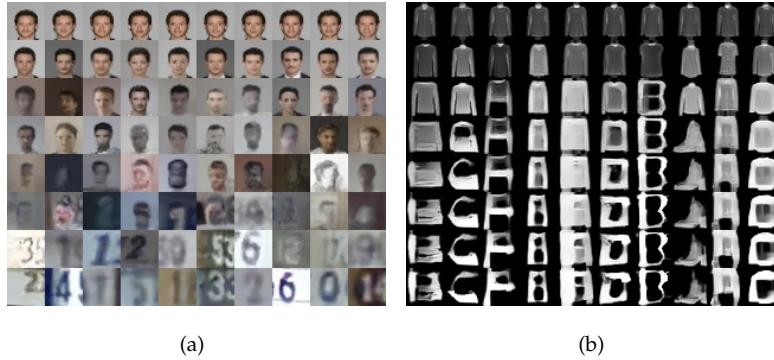


Fig. 13. (a) Train Glow on CelebA and sample from the fitted Gaussian of SVHN. (b) Train on FashionMNIST and sample from the fitted Gaussian of notMNIST. From top to down, the sampled noises from Gaussian are scaled by temperature 0, 0.25, 0.5, 0.6, 0.7, 0.8, 0.9, 1.0, respectively.

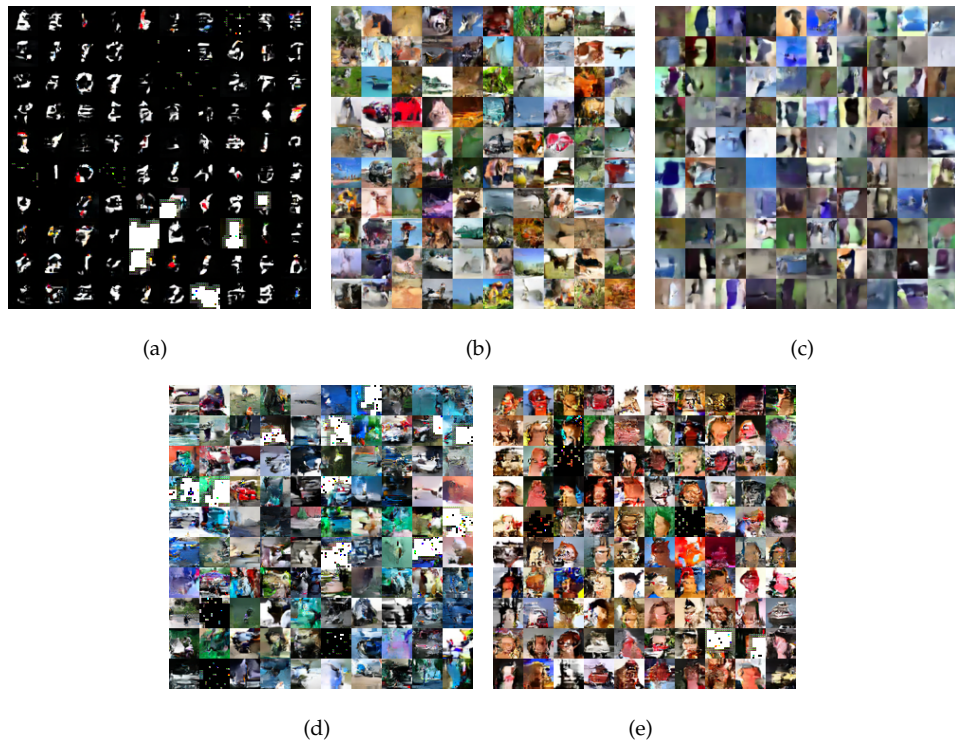


Fig. 14. Glow trained on CIFAR10. Generated images according to the fitted Gaussian from representations of (a) MNIST; (b) CIFAR100; (c) SVHN; (d) Imagenet32; (e) CelebA. We replicate MNIST into three channels and pad zeros for consistency. These results demonstrate that the covariance of representations contains important information of an OOD dataset.

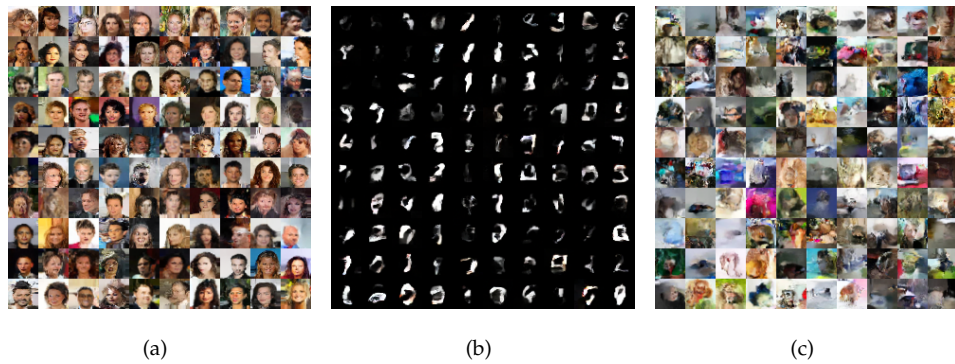


Fig. 15. Glow trained on CelebA32 $\times$ 32, sampling according to (a) standard Gaussian; (b) fitted Gaussian from MNIST representations; (c) fitted Gaussian from CIFAR10 representations.



Fig. 16. Glow trained on FashionMNIST. Sampling according to prior (up), fitted Gaussian from representations of MNSIT (middle) and notMNIST (down).

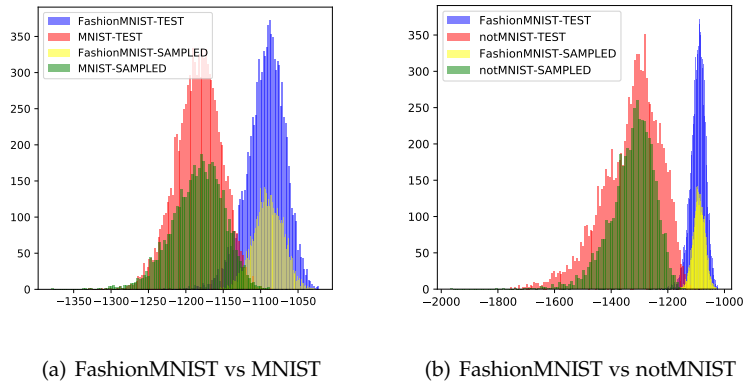


Fig. 17. Glow trained on FashionMNIST. Histogram of  $\log p(z)$  of (a) FashionMNIST vs MNIST, (b) FashionMNIST vs notMNIST under Glow. The green part corresponds to the  $\log p(z)$  of noises sampled from the fitted Gaussian of OOD datasets.

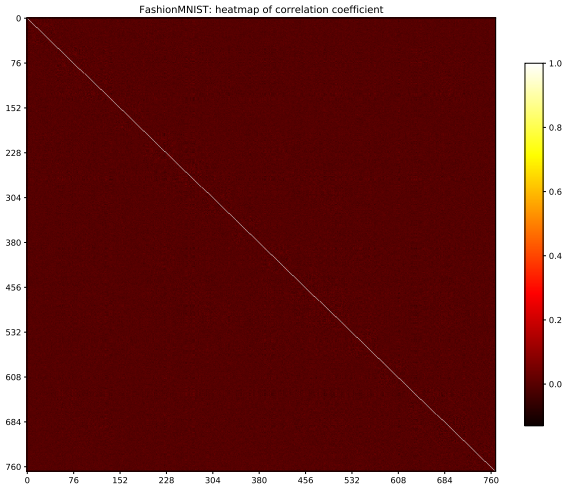


Fig. 18. Glow trained on FashionMNIST. Heatmap of correlation of FashionMNIST representations.

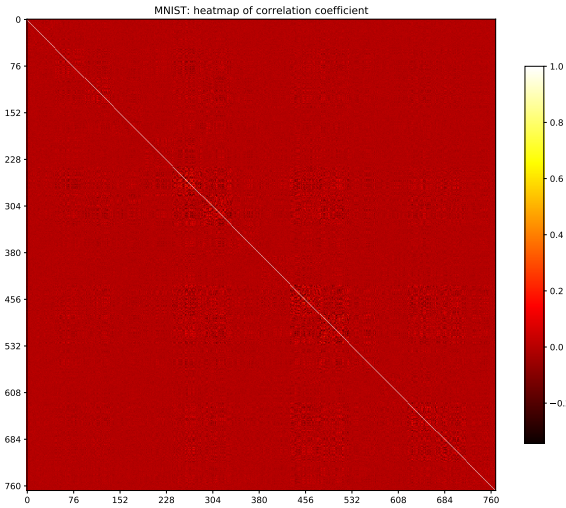


Fig. 19. Glow trained on FashionMNIST. Heatmap of correlation of MNIST representations.

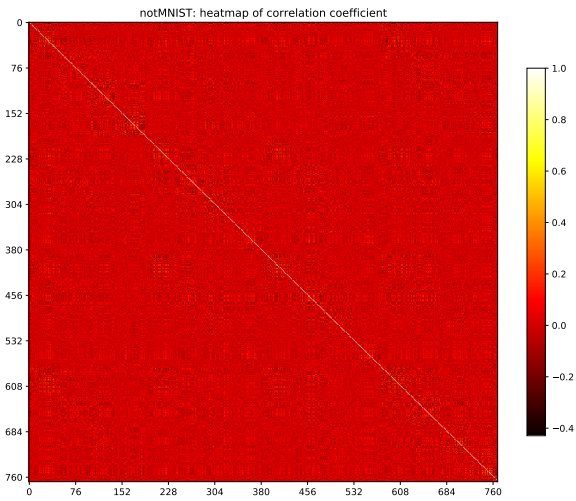


Fig. 20. Glow trained on FashionMNIST. Heatmap of correlation of notMNIST representations.

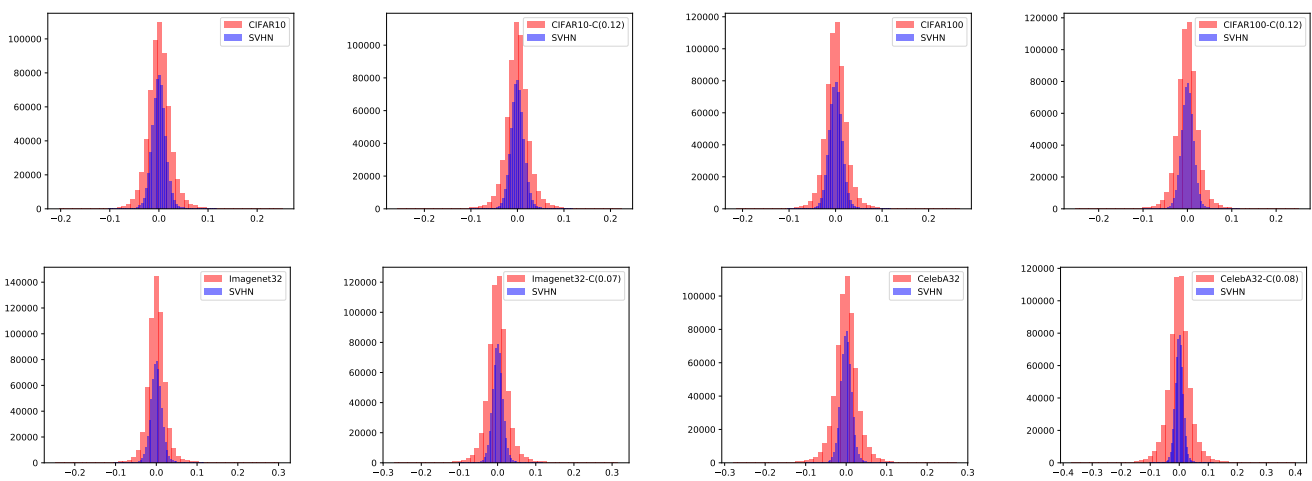


Fig. 21. Glow trained on SVHN. Histogram of non-diagonal elements of correlation of representations.



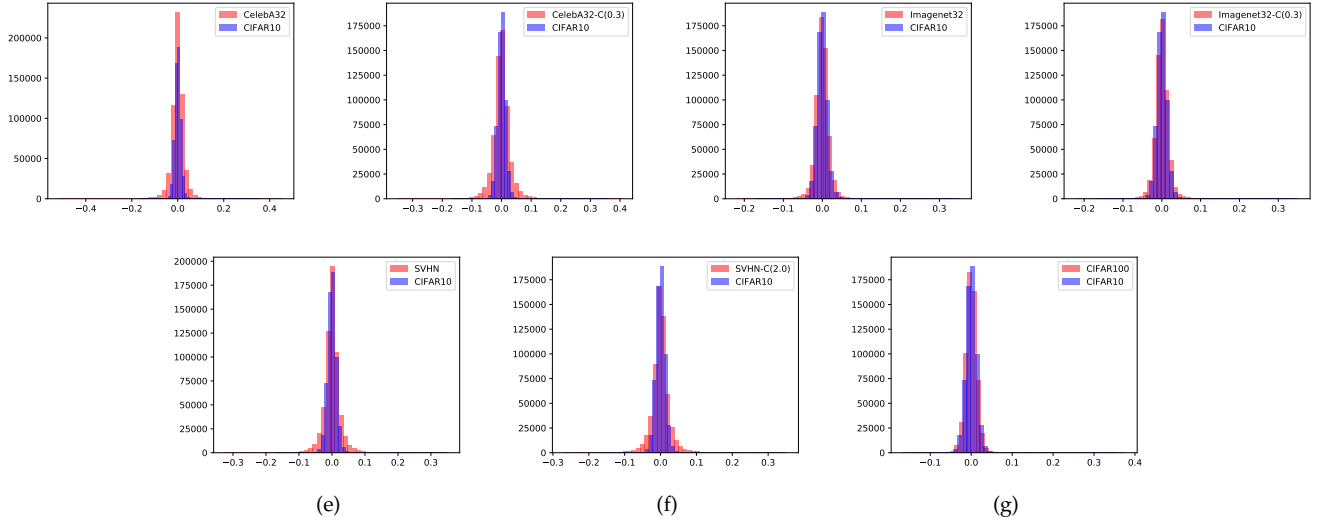


Fig. 22. Glow trained on CIFAR10. Histogram of non-diagonal elements of correlation of representations.

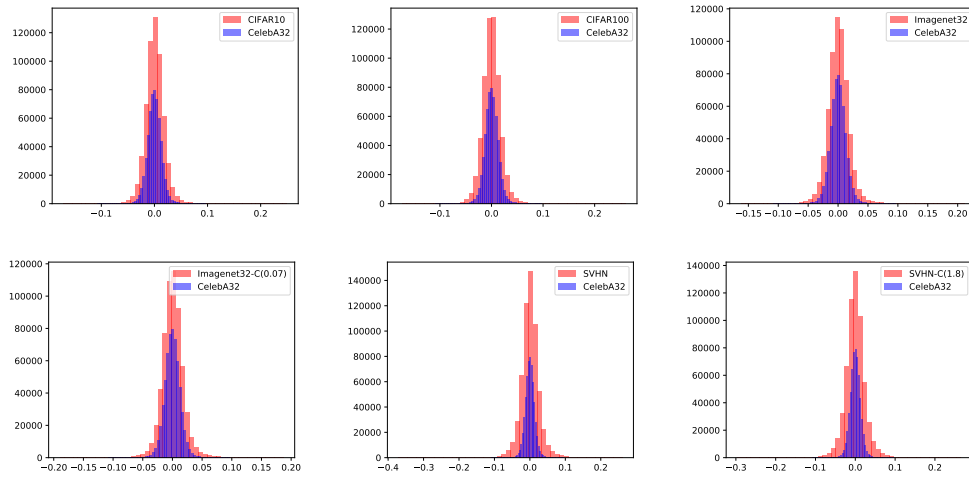


Fig. 23. Glow trained on CelebA. Histogram of non-diagonal elements of correlation of representations.

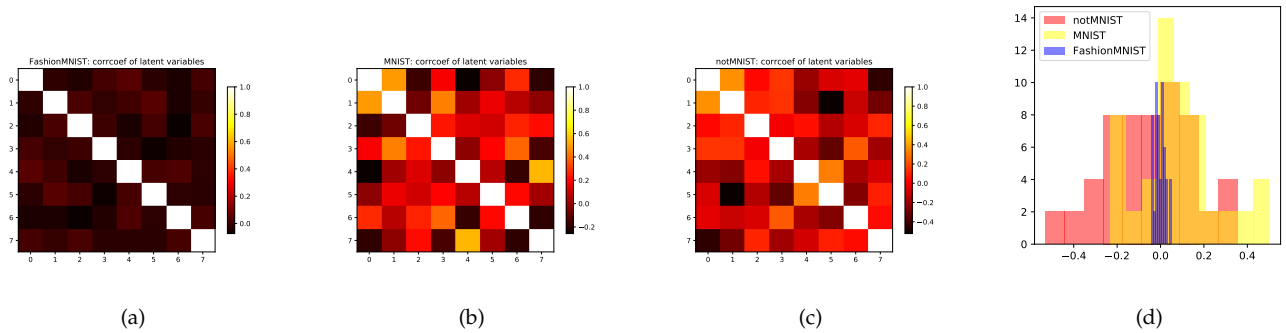


Fig. 24. VAE trained on FashionMNIST. Heatmap of correlation of (a)FashionMNIST (b)MNIST (c) notMNIST representations. (d) Histogram of non-diagonal elements of correlation of sampled representations.

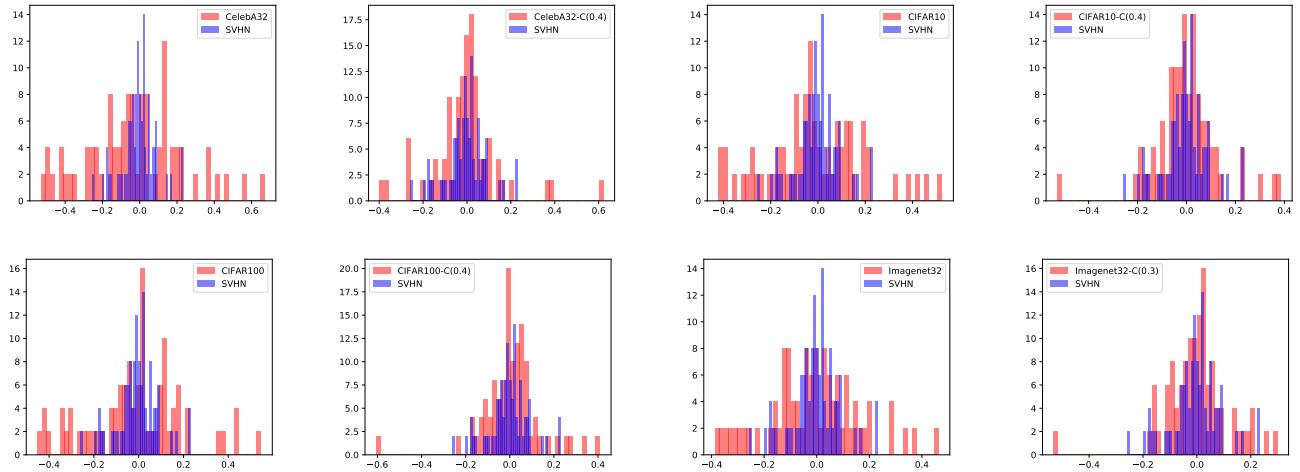


Fig. 25. VAE trained on SVHN. Histogram of non-diagonal elements of correlation of sampled representations.

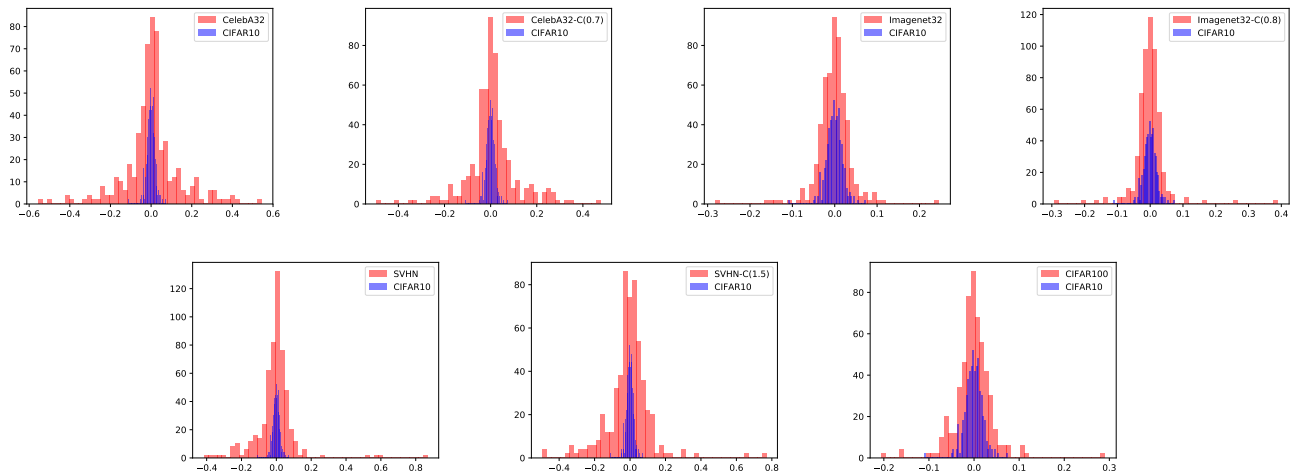


Fig. 26. VAE trained on CIFAR10. Histogram of non-diagonal elements of correlation of sampled representations.

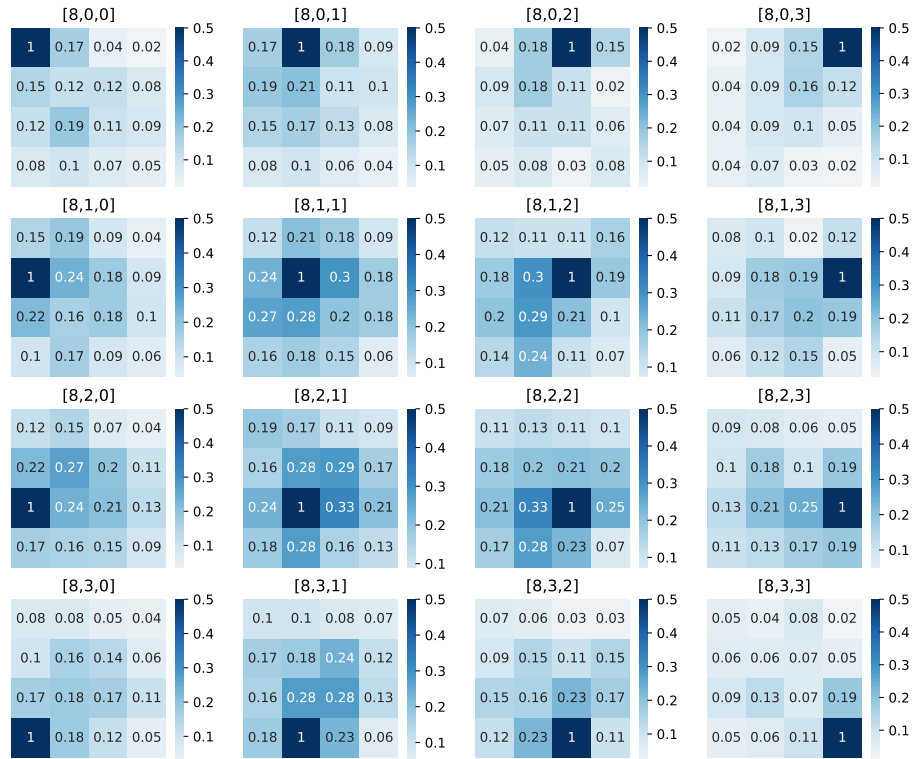
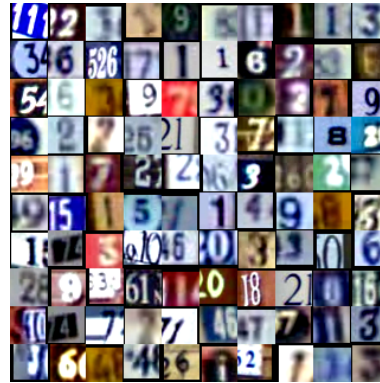


Fig. 27. Train Glow on SVHN and test on Imagenet32. We randomly select the 8-th channel. The subfigure at  $i$ -th row and  $j$ -th column shows the correlation between the pixel at position  $(i, j)$  and all other pixels. Adjacent pixels tend to have stronger correlation.



(a) SVHN



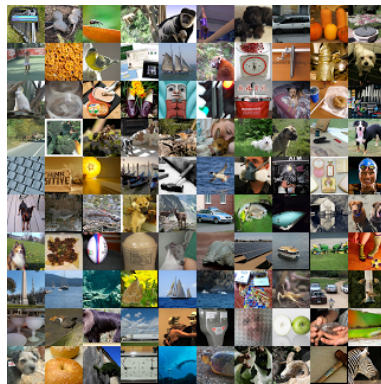
(b) SVHN with increased contrast by a factor of 2, have lower likelihood



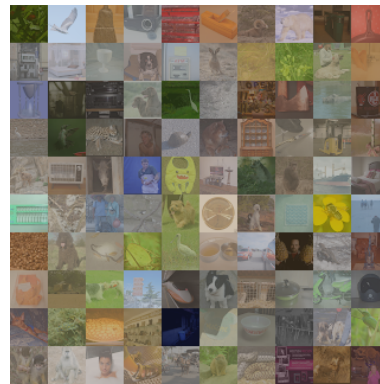
(c) CelebA32



(d) CelebA32 with decreased contrast by a factor of 0.3, have higher likelihood



(e) Imagenet32



(f) Imagenet32 with decreased contrast by a factor of 0.3, have higher likelihood

Fig. 28. Examples of datasets and their mutations. Under Glow trained on CIFAR10, these mutated datasets have the similar likelihood distribution with CIFAR10 test split.



Fig. 29. Generated images from Glow trained on (a) FashionMNIST; (b) CIFAR-10; (c) CelebA32.

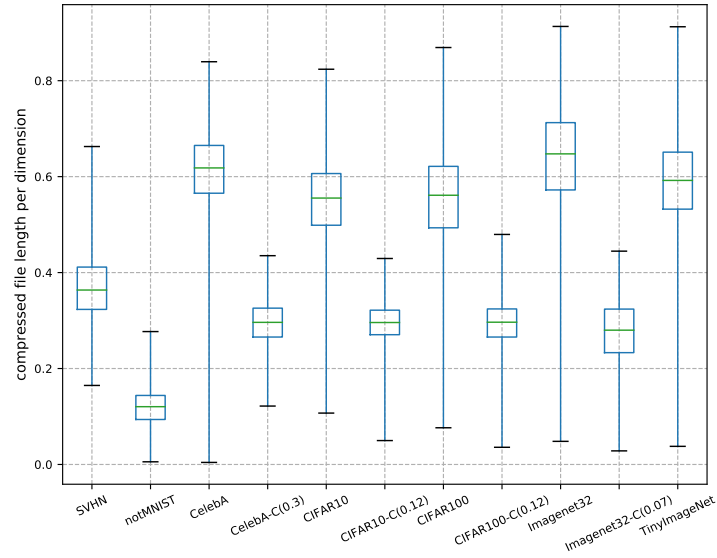


Fig. 30. The distributions of complexity estimated by the lengths of compressed files of data sets. We use FLIF as compressor and compute lengths in bits per dimension. Datasets with decreased contrast has lower complexity.